Annales Societatis Geologorum Poloniae (2020), vol. 90: 347–379 doi: https://doi.org/10.14241/asgp.2020.27

SEQUENCE ANALYSIS, CYCLOSTRATIGRAPHY AND PALYNOFACIES OF EARLY ANISIAN CARBONATE RAMP DEPOSITS, NW BULGARIA

George AJDANLIJSKY[1], André STRASSER[2] & Annette E. GÖTZ[3]*

[1] University of Mining and Geology "St. Ivan Rilski", Department of Geology and Geoinformatics, Sofia 1700, Bulgaria; e-mail: g.ajdanlijsky@mgu.bg
[2] University of Fribourg, Department of Geosciences, Geology-Palaeontology, 1700 Fribourg, Switzerland; e-mail: andreas.strasser@unifr.ch
[3] State Authority for Mining, Energy and Geology, 30655 Hannover, Germany; e-mail: annette.goetz@lbeg.niedersachsen.de
** Corresponding author*

Ajdanlijsky, G., Strasser, A. & Götz, A. E., 2020. Sequence analysis, cyclostratigraphy and palynofacies of early Anisian carbonate ramp deposits, NW Bulgaria. *Annales Societatis Geologorum Poloniae*, 90: 347–379.

Abstract: A sequence- and cyclostratigraphic interpretation of early Anisian (Aegean) shallow-marine carbonate ramp deposits, exposed in outcrop sections west of Tserovo village, NW Bulgaria, is presented. The hierarchical pattern identified can be interpreted in terms of Milankovitch cyclicity with elementary sequences representing the precession (20-kyr) cycle, small-scale sequences the short eccentricity (100-kyr), and medium-scale sequences the long eccentricity (400-kyr) cycle. Palynology provides a robust stratigraphic framework. The study of sedimentary organic matter, revealing variations of terrestrial input, sorting and fragmentation of phytoclasts, and prominent acritarch peaks, allows the interpretation of environmental changes and contributes to the cyclostratigraphic and sequence-stratigraphic framework. The detailed documentation of syndepositional soft-sediment deformation structures confirms their laterally traceable distribution within the depositional sequences and makes them good palaeoenvironmental indicators. Anisian ramp systems of the western Tethyan realm thus were subjected to highly dynamic regimes, recording the interplay between sea-level changes in tune with orbital cycles and ramp morphology.

Key words: Sedimentary cycles, palynofacies, Triassic, Western Balkanides, NW Bulgaria.

Manuscript received 04 August 2020, accepted 15 December 2020

INTRODUCTION

Anisian (Middle Triassic) carbonate ramp deposits of the northwestern Tethyan realm document a striking cyclicity in the stacking pattern of facies (Götz and Török, 2018). However, the lack of a robust biostratigraphic framework often hampers precise age control and thus regional correlation. Recent integrated palynological and sedimentological studies of the Anisian of NW Bulgaria (Ajdanlijsky *et al.*, 2018, 2019) enabled estimation of the timing of deposition and thus provide a better understanding of the ramp dynamics. This stratigraphic framework should be calibrated by studies across the ramp system, which is addressed here with a focus on the early Anisian shallow-marine deposits of the Iskar Carbonate Group, exposed in an excellent, continuous succession along the Iskar River gorge. In the Tserovo section presented here (Fig. 1), the early Anisian Opletnya Member (Mogila Formation) reaches a maximal thickness of 182 m – compared to 135 m in the type area – and is thus well suited to detailed study of the cyclic stratigraphic patterns and lateral facies variations, related to the ramp morphology.

In a previous paper, Ajdanlijsky *et al.* (2019) dealt with the sedimentological and cyclostratigraphic analysis of the Mogila Formation in two sections (Lakatnik and Sfrazen; Fig. 1B). Here the authors go a step further by applying the same methodology to the nearby Tserovo section (Fig. 1C), which allows refinement of the palaeoenvironmental and stratigraphical interpretation of this Middle Triassic carbonate ramp.

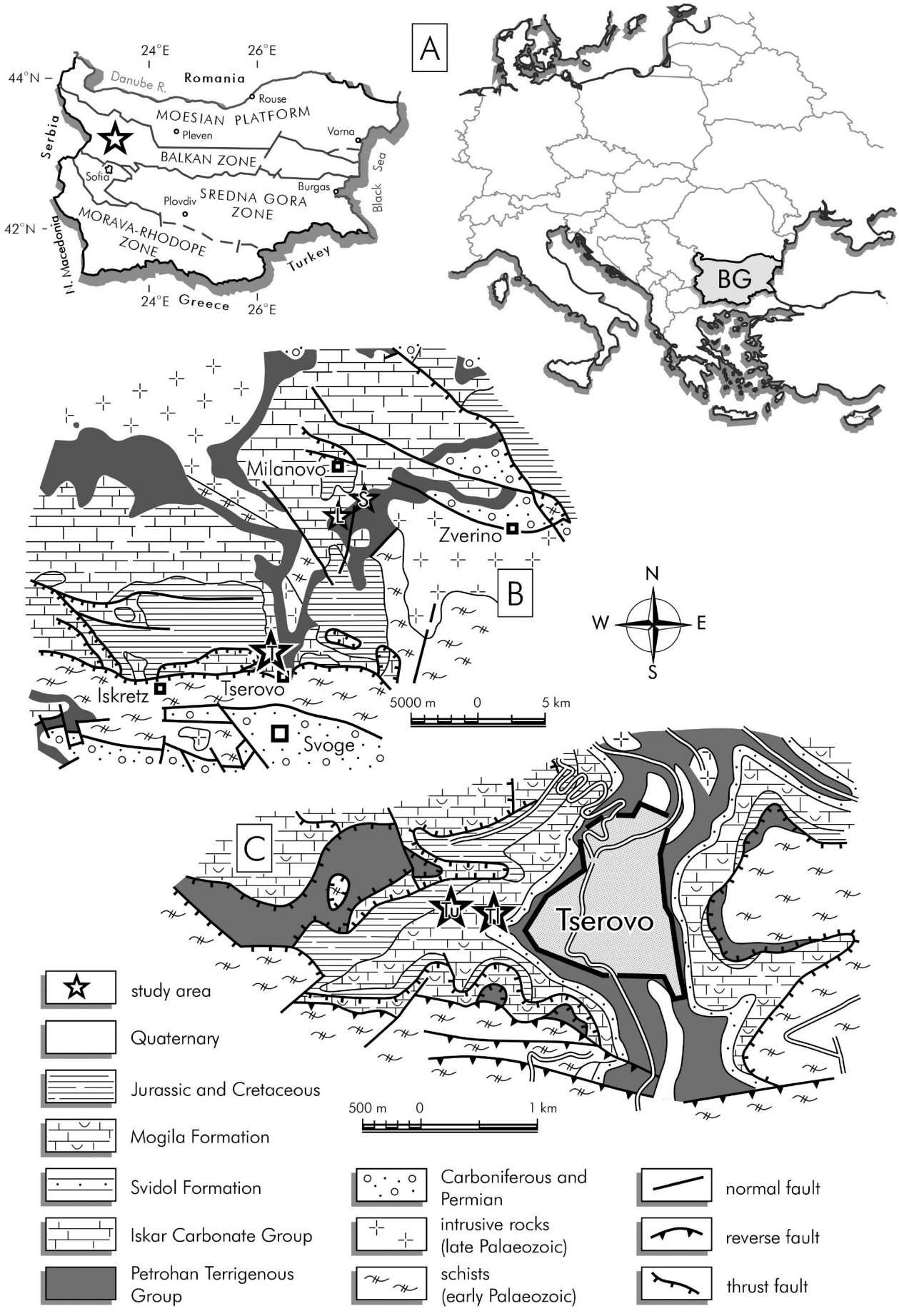

Fig. 1. Study area and location of the Tserovo section studied (Tl: lower part, Tu: upper part). L: Lakatnik section; S: Sfrazen section. **A.** Schematic structural map of Bulgaria. **B.** Geological map of part of the Western Balkan Zone. **C.** Southern flank of the Berkovitza Unit.

GEOLOGICAL SETTING

The study area is part of the Western Balkanides, the so-called Western Balkan Tectonic Zone (Ivanov, 1998) of the Alpine orogenic belt, dominated by Mesozoic sedimentary rocks (Fig. 1). The Lower Triassic Petrohan Terrigenous Group (Tronkov, 1981) consists predominantly of fluvial deposits, overlain by the Iskar Carbonate Group (Tronkov, 1981), composed of shallow-marine carbonates and assigned to the Anisian stage. The present study concerns the Opletnya Member of the Mogila Formation (Fig. 2). Lower Jurassic clastic rocks cover the Triassic succession with a marked disconformity.

The pre-Mesozoic basement includes lower Palaeozoic high-grade metamorphic rocks and upper Palaeozoic intrusive and volcanic rocks. Together with Triassic rocks, they are arranged as a set of overthrusts and thrust faults (Yanev, 2000).

MATERIALS AND METHODS

The Tserovo section studied exposes the uppermost Petrohan Terrigenous Group and the lower part of the Iskar Carbonate Group (Fig. 2). The total thickness of the succession reaches 182 m. Its lower part (about 98 m) is located 80 m northwest of the village of Tserovo and the upper part (110 m) is about 450 m to the west (Fig. 1C). The two parts were logged with a 26 m overlap in order to ensure correlation. A detailed bed-by-bed documentation was performed including lithology, fossil content, and sedimentary structures. Furthermore, the lateral development and amplitude of distinct erosional surfaces and levels with syndepositional soft-sediment deformations were studied. The prevailing direction of sedimentary palaeotransport were studied by measurement of cross-bedding orientation. The microfacies and the textures (classification according to Dunham, 1962) were determined on the outcrop with a hand lens and in 155 lithological samples including 92 thin-sections. A total of 19 samples for palynostratigraphy were taken from the uppermost Petrohan Terrigenous Group and the Svidol and Mogila formations (basal Iskar Carbonate Group). Two elementary sequences within the lower Mogila Formation (Opletnya Member) were sampled for high-resolution palynofacies analysis.

Palynological samples were prepared using standard processing techniques (Wood *et al.*, 1996), including HCl (33%) and HF (73%) treatment for the dissolution of carbonates and silicates, and saturated $ZnCl_2$ solution ($D \approx 2.2$ g/ml) for density separation. Residues were sieved at 15-µm mesh size and mounted in Eukitt, a commercial, resin-based mounting medium. Palynological slides were analyzed under a Leica DM2000 microscope. Palynofacies analysis was performed dividing the sedimentary organic matter into a marine (autochthonous) fraction of marine phytoplankton and foraminiferal test linings and a continental (allochthonous) fraction of pollen grains, spores, and phytoclasts. The palynofacies parameters that were used to decipher transgressive-regressive trends within the studied succession are: (1) the ratio of continental to marine constituents (CONT/MAR); (2) the ratio of opaque to translucent phytoclasts (OP/TR); (3) the phytoclast particle size and shape (equidimensional to blade-shaped: ED/BS); and (4) the relative proportion and species diversity of marine phytoplankton.

PALYNOSTRATIGRAPHY

Palynological investigations in the Triassic of Bulgaria focused on the age assignment of formations (Kalvacheva and Čatalov, 1974; Čatalov and Visscher, 1990; Petrunova, 1992a, b, 1999, 2000; Budurov *et al.*, 1997). Recently, palynological studies on continental and marine deposits of the Early–Middle Triassic transition interval exposed in outcrops along the Iskar River gorge (Ajdanlijsky *et al.*, 2018) enabled the placement of the Olenekian–Anisian boundary in the uppermost fluvial Petrohan Terrigenous Group. Within the Anisian, the identification of three palynoassemblages (Ajdanlijsky *et al.*, 2019) provided a high-resolution stratigraphic scheme that is applied in the present study.

Anisian key taxa appear in the lowermost Svidol Formation (Fig. 2) including *Cristianisporites triangulatus* Antonescu, *Illinites kosankei* Klaus, *Illinites chitonoides* Klaus, *Stellapollenites thiergartii* (Mädler) Clement-Westerhof, Van der Eem, Van Erve, Klasen, Schuurman & Visscher, *Tsugaepollenites oriens* Klaus, and *Triadispora crassa* Klaus. Early Triassic elements, such as *Densoisporites nejburgii* (Schulz) Balme and *Voltziaceaesporites heteromorphus* Klaus, are still present, indicating an early Anisian (Aegean) age (Palynoassemblage I; Ajdanlijsky *et al.*, 2019). The first marine acritarchs were recorded from the basal Mogila Formation. In the upper Opletnya Member of the Mogila Formation, Anisian taxa as listed above are present, lacking Early Triassic elements. This observation is in accordance with the findings of the early Anisian succession, exposed in the neighboring Lakatnik and Sfrazen sections (Ajdanlijsky *et al.*, 2019) that are situated about 14 km to the north of the Tserovo sections. A Bithynian age is thus assigned to the upper Opletnya Member (Palynoassemblage II; Ajdanlijsky *et al.*, 2019).

SEDIMENTOLOGY

The section of the Opletnya Member, studied near Tserovo village, is dominated by wacke- and mudstones with only few dolostones. Pack- and grainstones are present, but only in a few horizons. Marls and dolomarls, claystones, and fine-grained siliciclastic rocks are very rare.

Wackestones and mudstones

Wacke- and mudstones are medium- to thin-bedded (5–30 cm), rarely thick-bedded (50–95 cm; Fig. 3; elementary sequences 20 and 24), often massive, also laminated, nodular or platy (Fig. 4C). Most of the nodular and platy type is connected with increased clay content. Laminations are 1 to 3 mm thick (Fig. 4A). The beds contain benthic foraminifera, bivalves, echinoderms and peloids (Fig. 5A, C, D, E). A few scattered brachiopods and gastropods are also present (Fig. 5B, C). Terrigenous components are represented by silt and clay and some mudstone beds contain organic

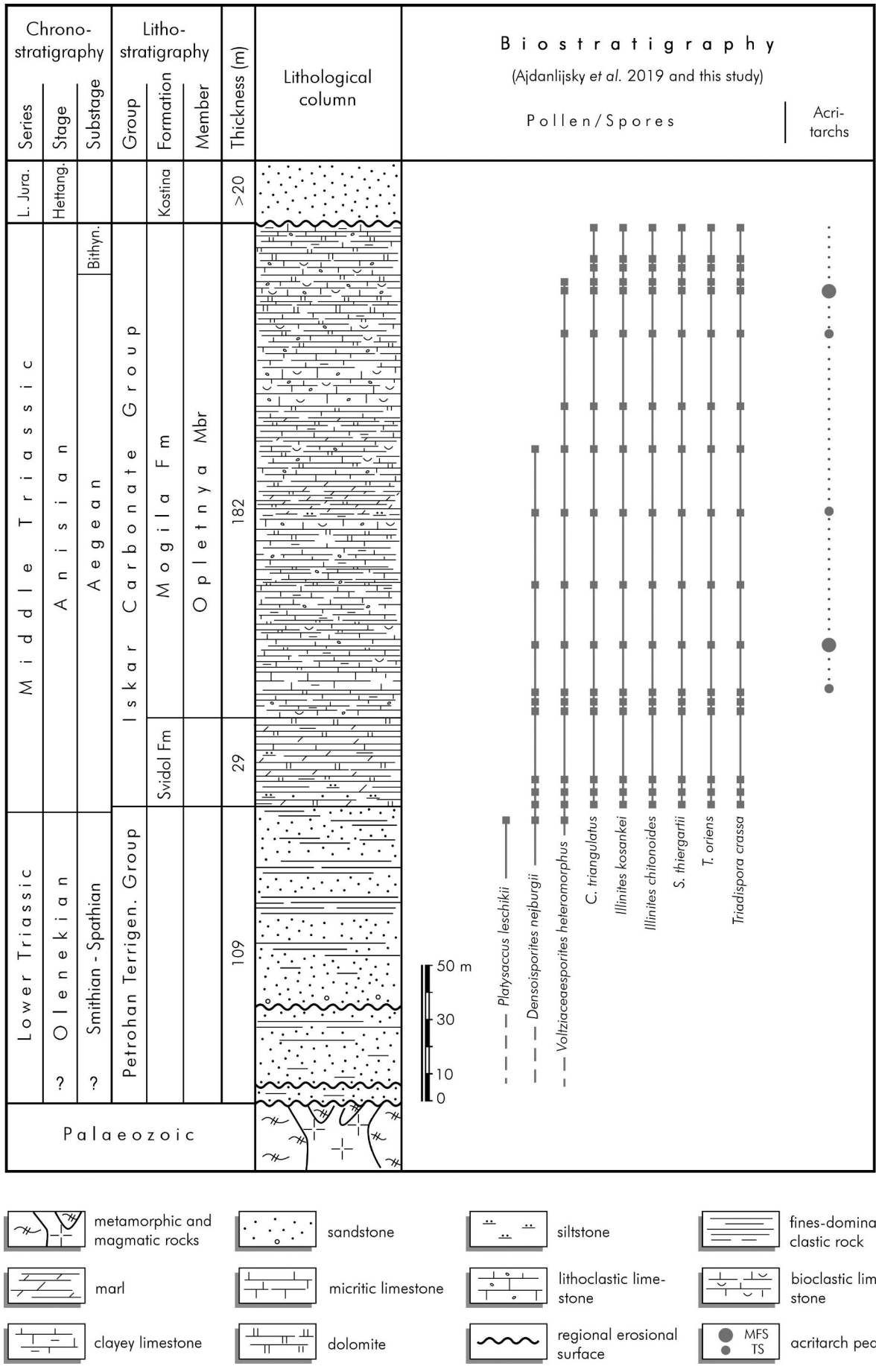

Fig. 2. Stratigraphy of the Middle Triassic sequence exposed in the outcrop section studied with the position of the Olenekian–Anisian boundary based on new biostratigraphic data. Acritarch peaks mark major transgressive (TS) and maximum-flooding (MFS) phases.

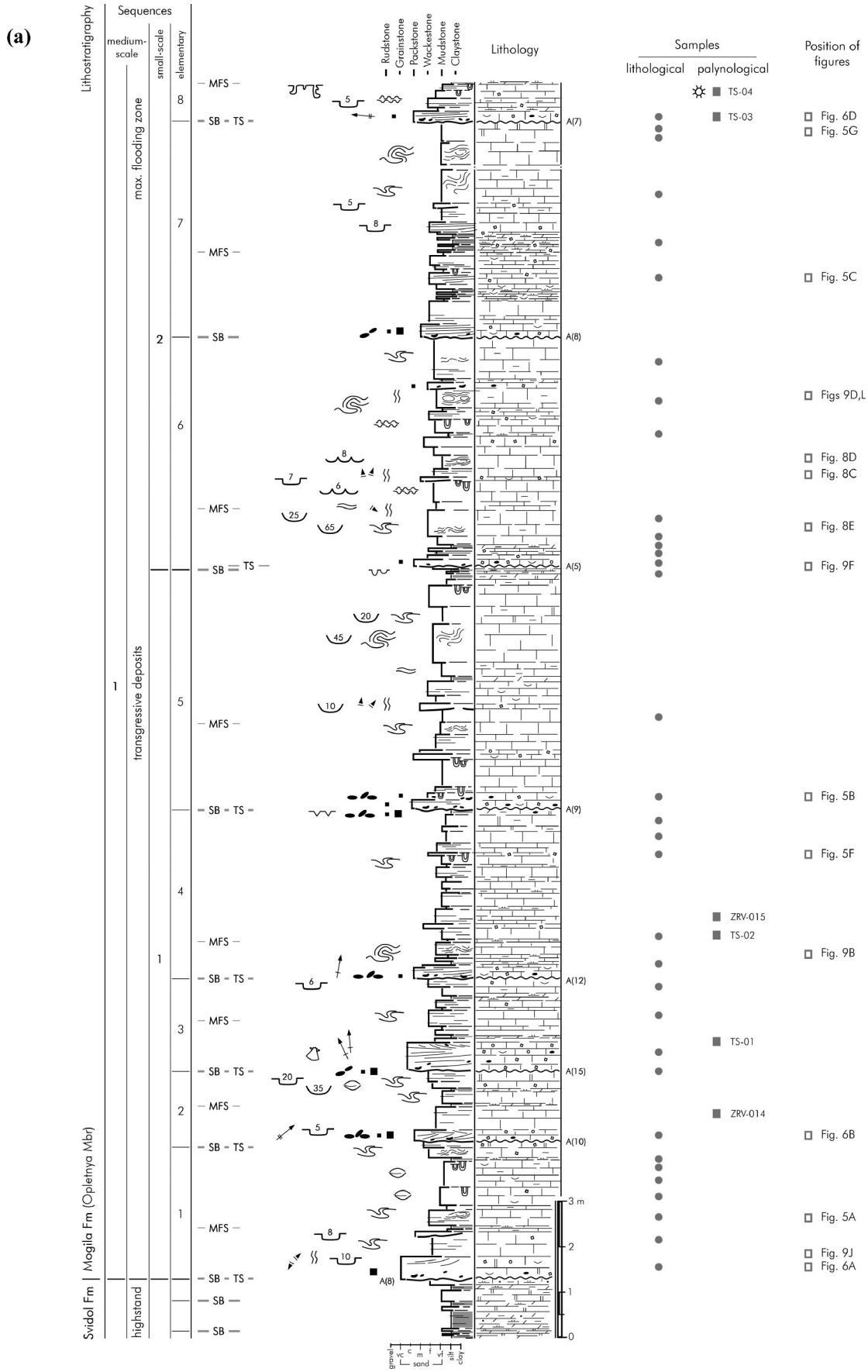

Fig. 3. Sequence- and cyclostratigraphic interpretation of the Opletnya Member (Mogila Formation) in the studied Tserovo sections. **A.** Transgressive and maximum-flooding phase of medium-scale sequence 1. **B.** Highstand phase of medium-scale sequence 1. **C.** Highstand phase of medium-scale sequence 1 and transgressive and maximum-flooding phase of medium-scale sequence 2. **D.** Highstand phase of medium-scale sequence 2. **E.** Transgressive and maximum-flooding phase of medium-scale sequence 3. **F.** Highstand

(b)

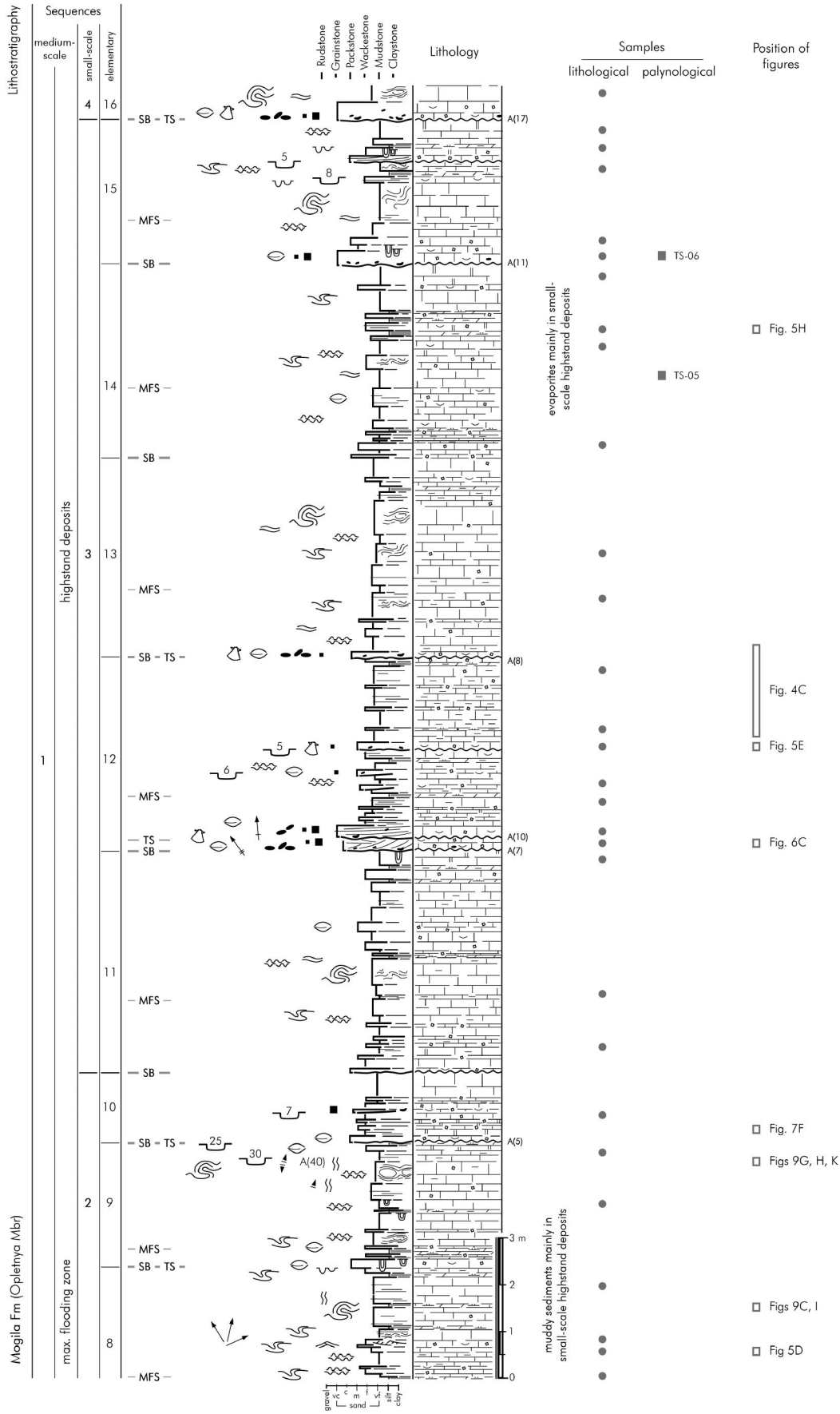

phase of medium-scale sequence 3, medium-scale sequence 4, and transgressive phase of medium-scale sequence 5. **G.** Maximum-flooding and highstand phase of medium-scale sequence 5. The maximum amplitude is indicated for the most prominent erosional surfaces. SB: sequence boundary; TS: transgressive surface; MFS: maximum-flooding surface.

(c)

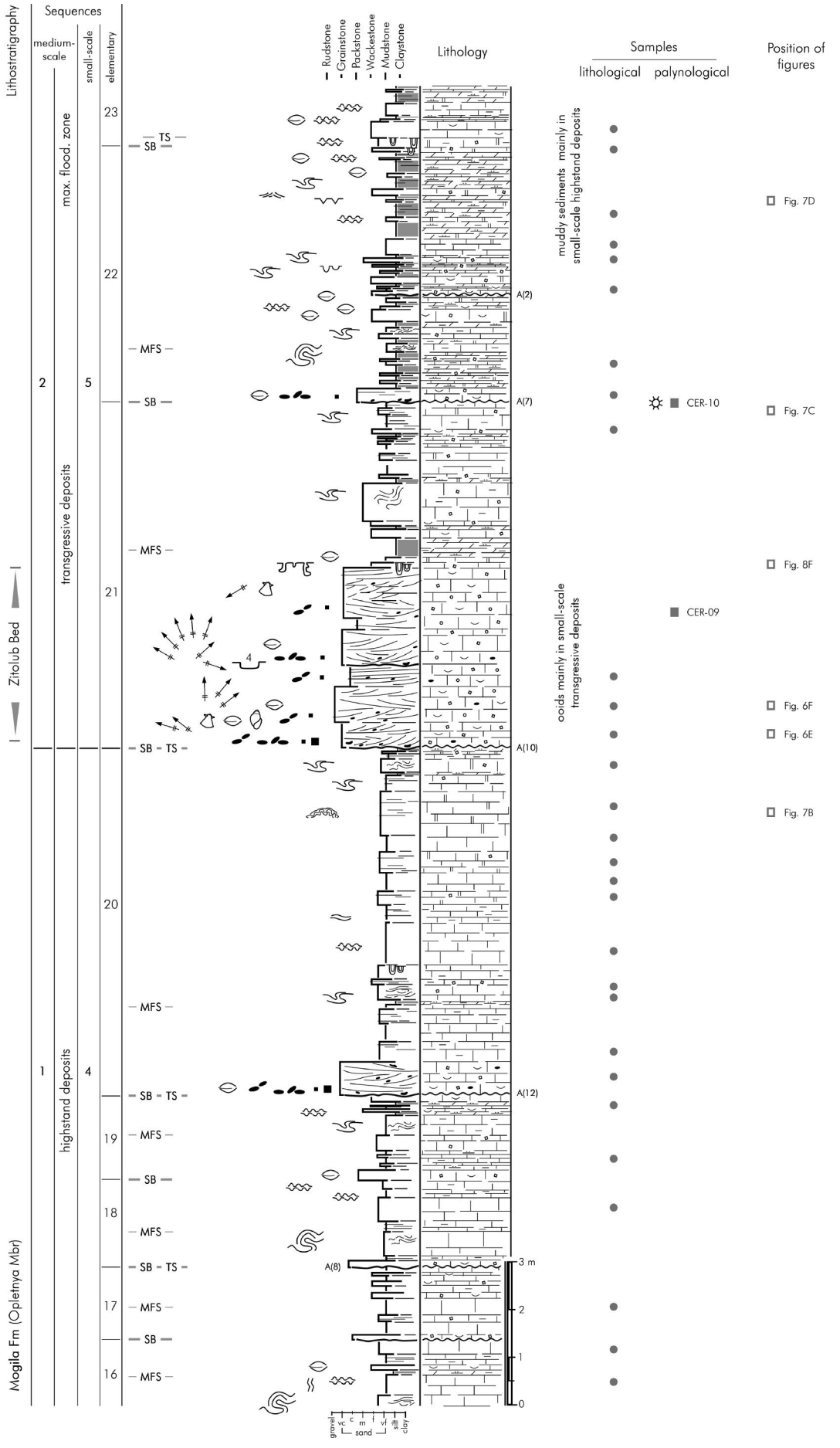

Fig. 3. continued.

(d)

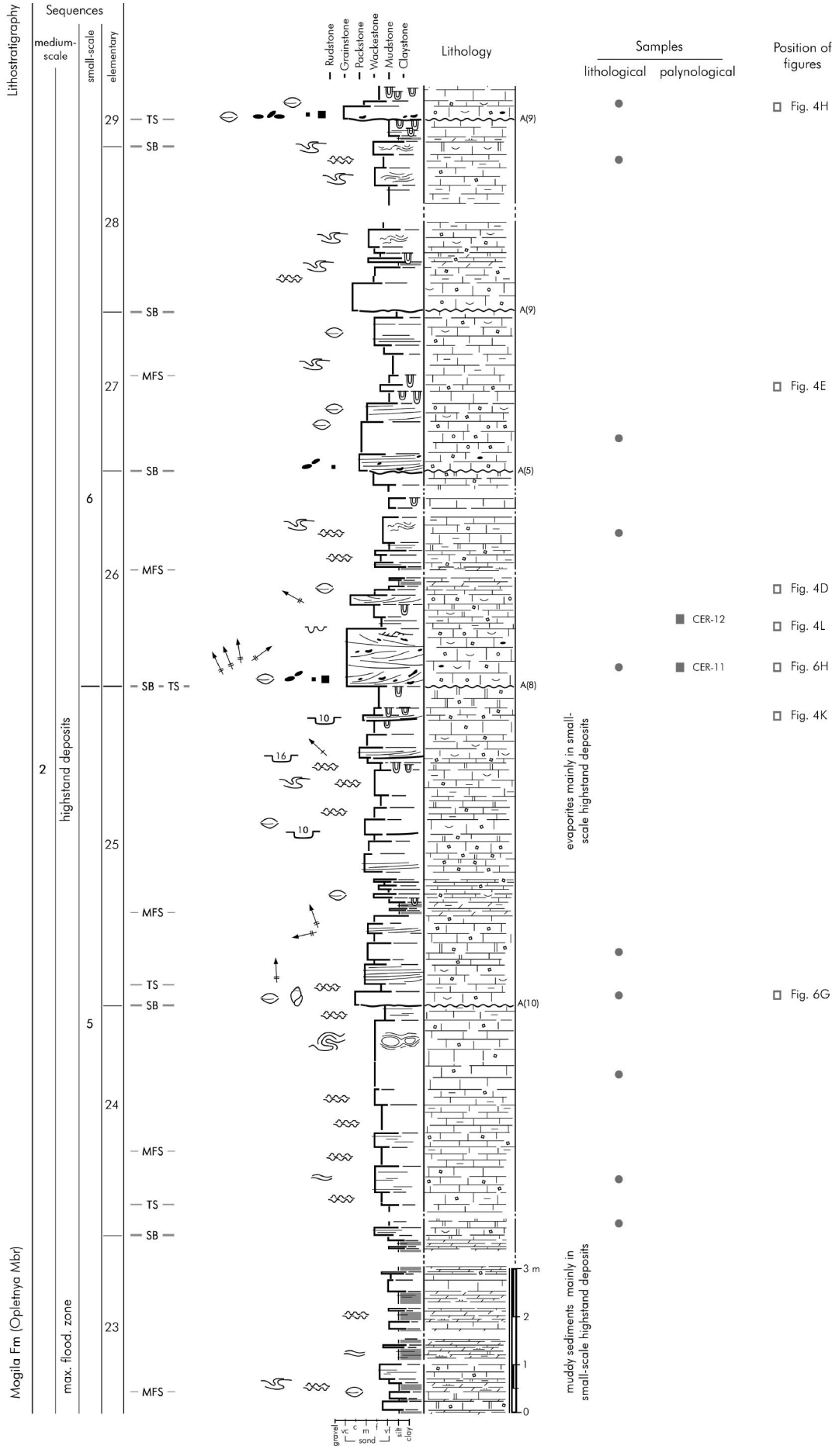

Fig. 3. continued.

(e)

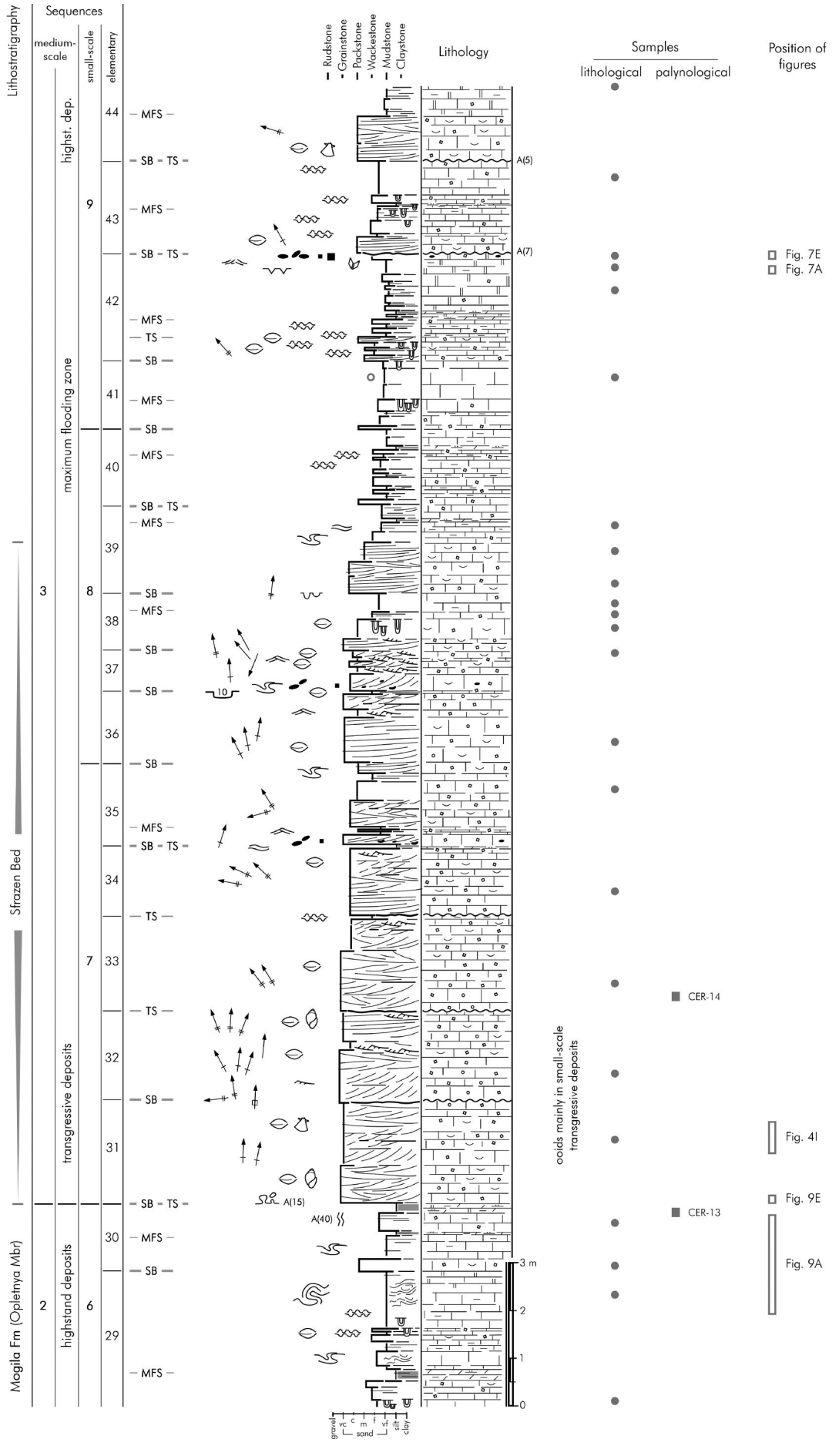

Fig. 3. continued.

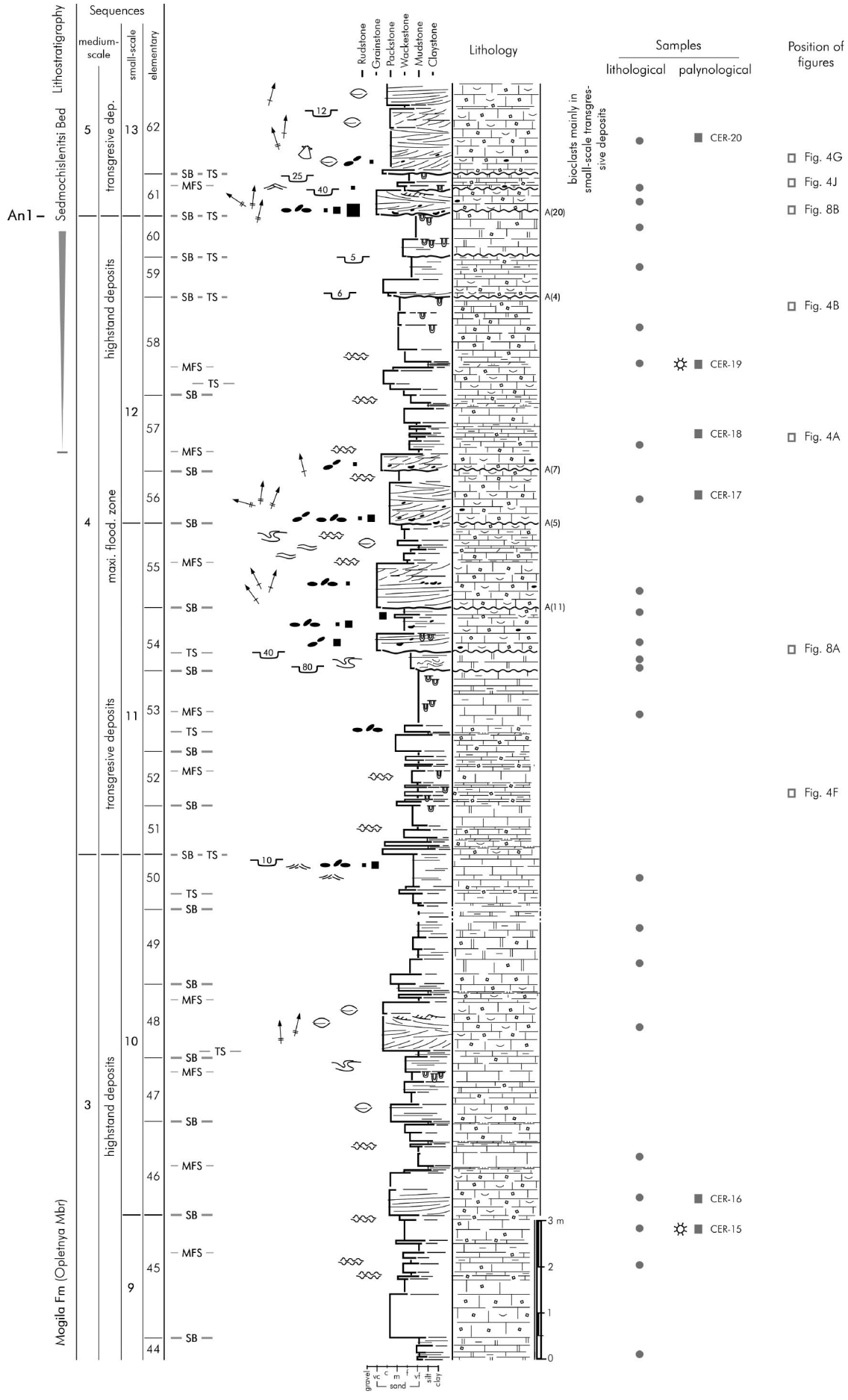

Fig. 3. continued.

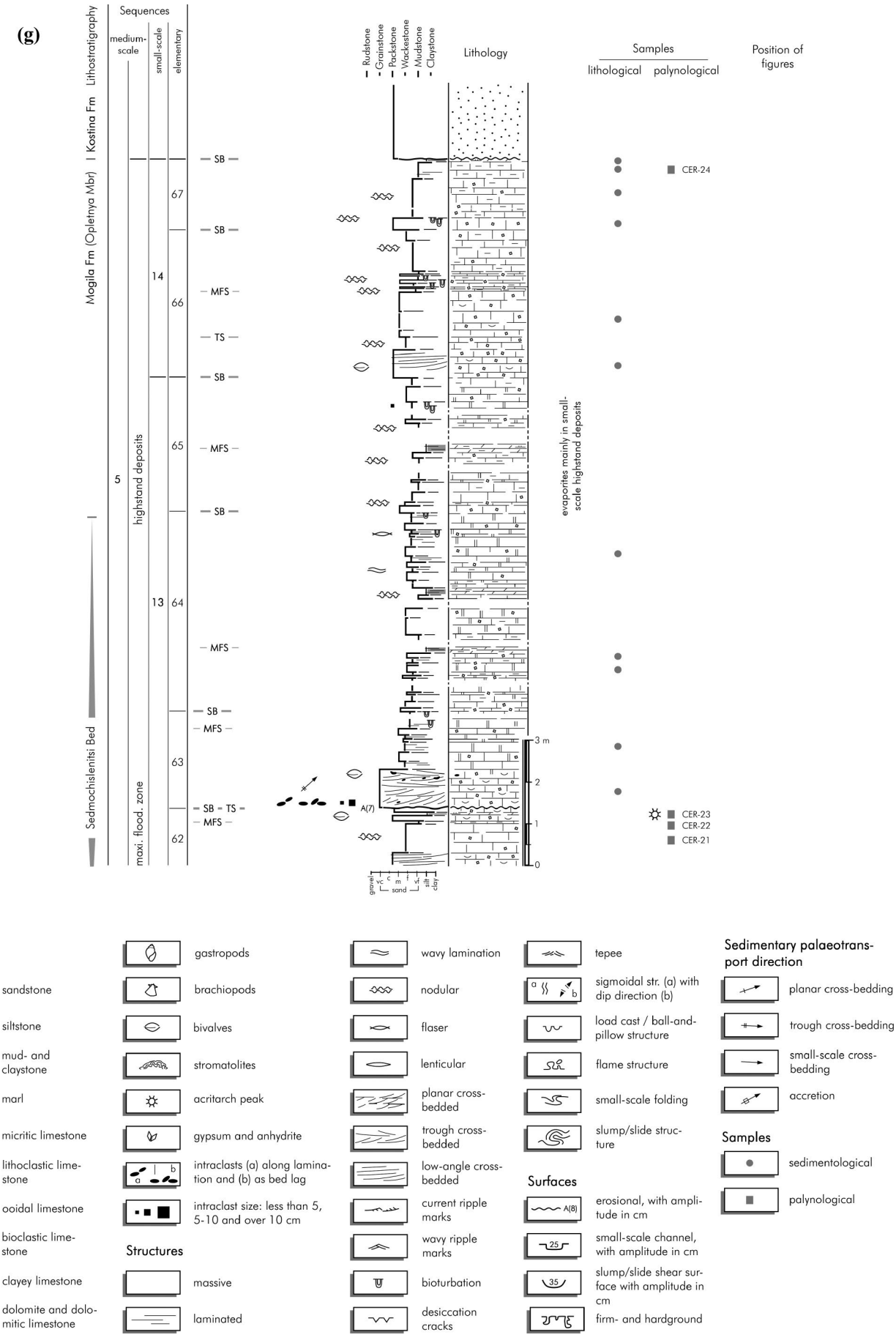

Fig. 3. continued.

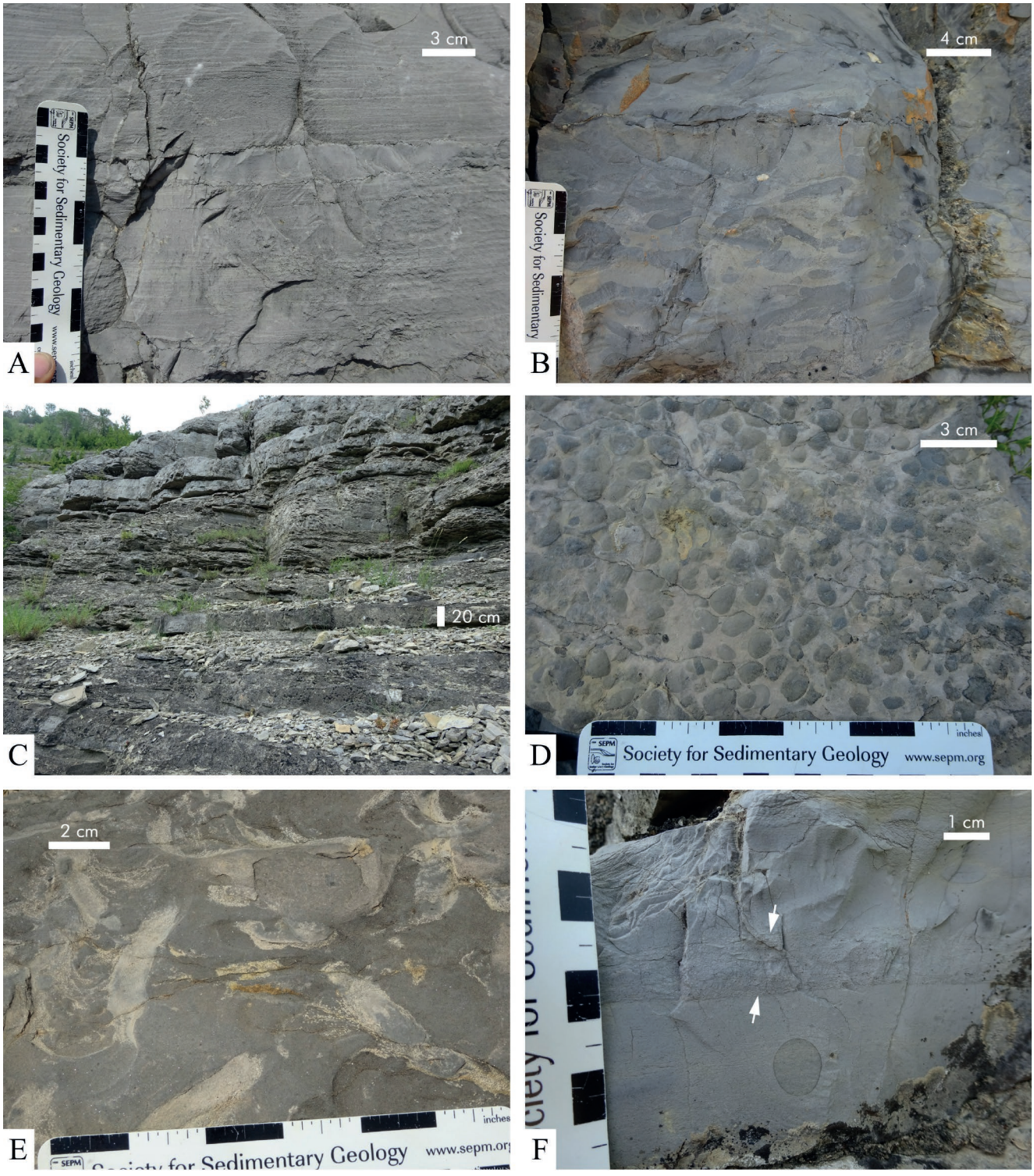

Fig. 4. Limestone lithologies. **A.** Millimetre-laminated wackestone, palynological sample CER-18, elementary sequence 57. **B.** Dolomitized, intensively bioturbated wackestone from the uppermost part of elementary sequence 58. **C.** Over 2 m thick interval of laminated clayey mud- and wackestones between limestone beds, displaying wavy bedding, elementary sequence 12. **D.** Plane view of bivalve shell bed below the maximum-flooding surface of elementary sequence 26. **E.** Strongly bioturbated (*Rhizocorallium commune*) mudstone at the maximum-flooding surface of elementary sequence 27. **F.** Storm-generated thin bed (tempestite – between arrows) with normal grading from pack- to wackestone developed in the mudstone-dominated upper part of elementary sequence 52. **G.** Massive

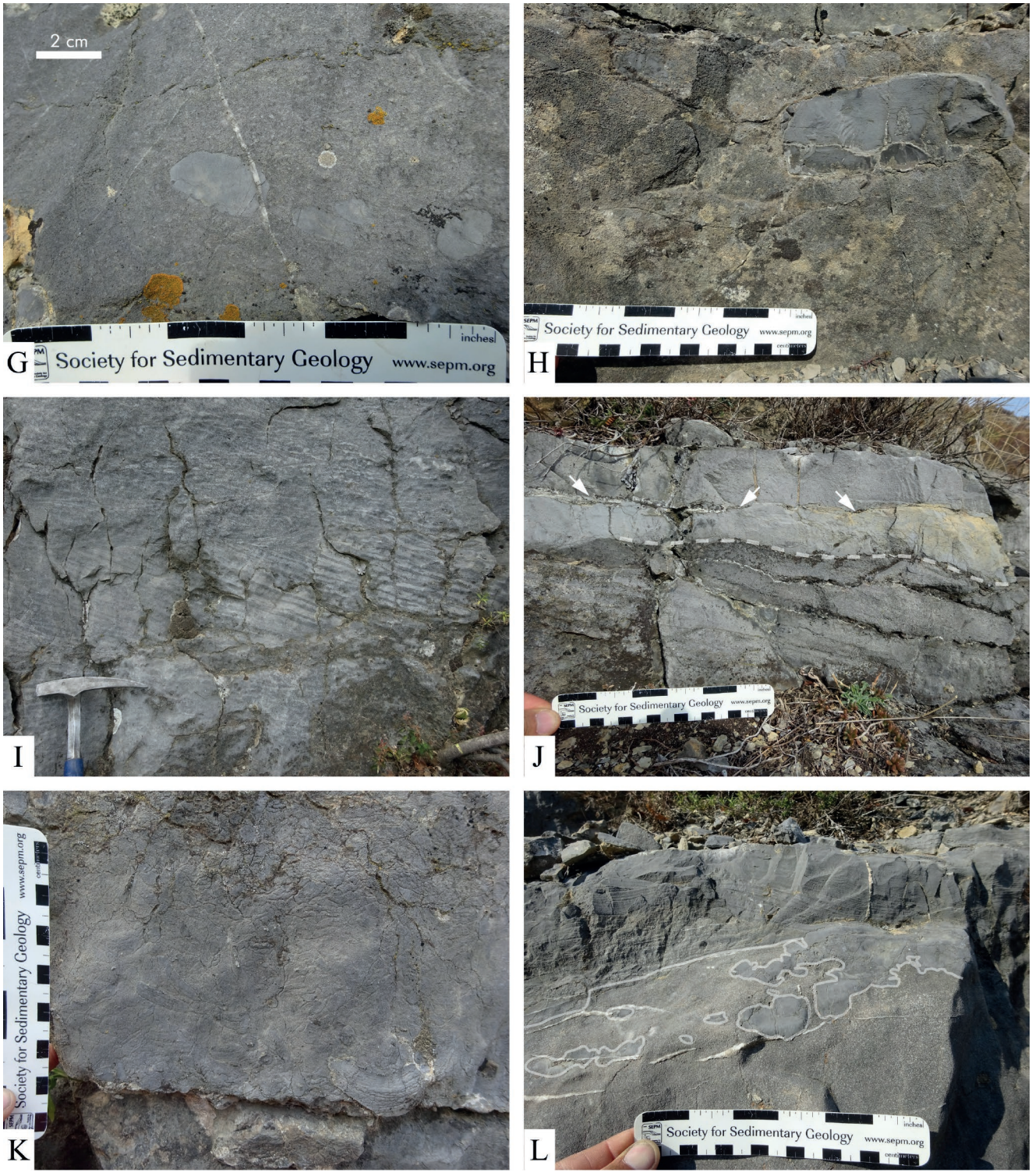

bioclastic packstone with rounded wackestone intraclasts, elementary sequence 62. **H.** Coarse-grained ooidal grainstone with sub-angular mudstone intraclasts, elementary sequence 29. **I.** Planar and trough cross-bedded grainstone; lower part of the Sfrazen Bed, elementary sequence 31. **J.** Planar-bedded grainstone (below dashed line – small-scale accretion surface) overlain by symmetric climbing ripples (below arrows), followed by bioturbated dolo-wackestone, elementary sequence 61. **K.** Strongly bioturbated pack- to wackstone filling a small erosional channel in the upper part of elementary sequence 25. **L.** Ball-and-pillow structures (outlined) of laminated mud- to wackestone overlain by cross-bedded packstone, highstand of elementary sequence 26. The numbering of the elementary sequences is as in Figure 3.

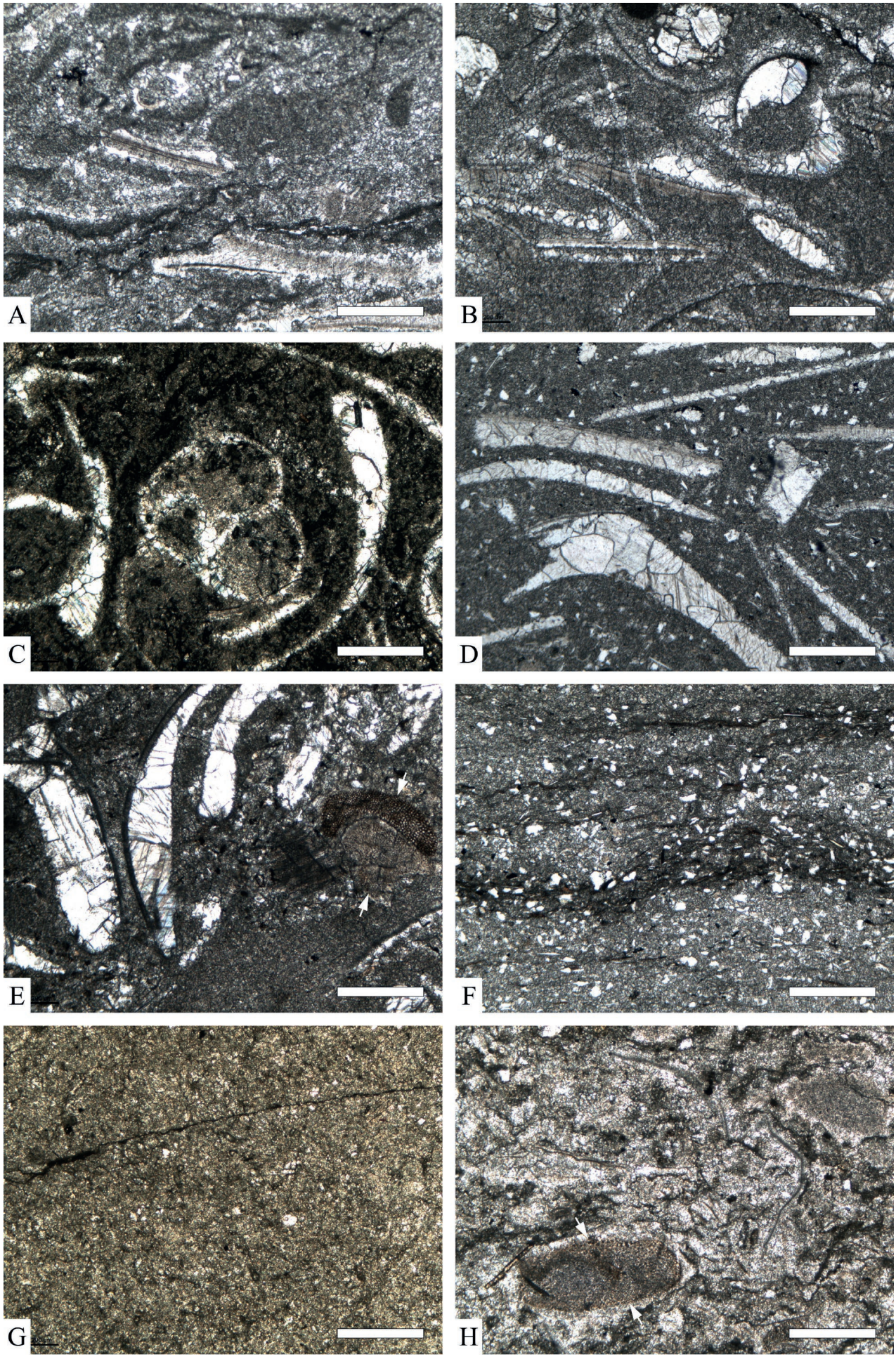
A
B
C
D
E
F
G
H

matter (Fig. 5F). At several levels, very thin bivalve beds or lenses were documented (Fig. 4D).

Some beds contain thin (5–7 mm) layers, grading from pack- to wackestone, with a sharp erosional base that can be traced laterally (Fig. 4F). These layers are interpreted as a result of storm events and thus classified as tempestites, albeit in very shallow-water environments. Tepees and flat-pebble lags are very rare (Fig. 3; elementary sequence 50). In the middle and upper part of the section, wacke- and mudstones are dolomitized and locally show intervals of intense bioturbation (Fig. 4B, E).

Syndepositional, soft-sediment deformation structures of different scales and morphologies were observed in the wacke- and mudstones. Load casts and ball-and-pillow structures are among the most common features and occur mainly along the boundaries between these two lithologies and in cases where coarser-grained rocks cover fines (see Fig. 9F). Opposite cases were also observed, where this structure is developed at the top of coarser-grained (mostly packstone) beds, overlain by finer-grained beds (Fig. 4L). Other syndepositional deformation structures include sigmoids, folds and ball-and-pillow, connected with erosion, sliding, and slumping; these are described in detail below. Often, they are connected with marked shear surfaces or dm-scale local channels.

Although wacke- and mudstones are common throughout the studied section, they predominate in its lower part, below the Sfrazen Bed, where wacke- and mudstones form 3–4 m thick packages (Fig. 3; elementary sequences 7, 13 and 14). Mudstones mark the quietest sedimentary environments, with restricted water circulation, where bioturbation may be intense.

Packstones and grainstones

Peloids, bioclasts, and ooids are the typical components of the pack- and grainstones in the section studied (Fig. 6A, B, E, F, H). Bioclasts are mainly bivalve and gastropod shells (Fig. 6B, D, G), and fragments of echinoderms and benthic foraminifera are present (Fig. 6B, C). Intraclasts occur in the bottomset beds and cover the foreset surfaces of cross-beds (Fig. 4G). According to their surfaces, two different types of intraclasts are recognized: intraclasts with sharp surfaces (Fig. 4H) and intraclasts showing poorly defined surfaces with gradual transition into the hosting material (Fig. 4G). While the first type is a typical product of reworking and redeposition of well-lithified materials, the second one is interpreted as resulting from resedimentation of semi-lithified material, or from the incipient disintegration of semi-consolidated beds (Ajdanlijsky *et al.*, 2019). Intraclast lag deposits and imbrication structures are locally developed (Fig. 3; elementary sequences 11–12, 20–21, 28, 42, 54–56, 61, 63).

Massive beds are more common in the lower parts of the section, below the Sfrazen Bed, while cross-bedded units – low-angle, planar, and trough type – are more often developed in its upper part (Fig. 4I). The lamination is mm- to cm-thick (Fig. 4I, J). Accretion and reactivation surfaces are present, planar bedding and trough cross-bedding are equally represented. Small-scale cross-bedding is less developed and occurs mainly in the upper part of the section. Wavy bedding (Fig. 4C) occurs more often than current ripples. The set thickness ranges from a few cm to a few tens of cm, while thicknesses of the co-sets may reach several metres. Bioturbation occurs in most of the beds (Fig. 4K). Partial dolomitization of the packstones is developed in the lowermost part of the section.

The orientation of the cross-bedding structures was measured as an indicator for the palaeotransport direction and sedimentary setting. Although the cross-bedding direction measured varies over a wide range within one co-set (e.g., in the Zitolub Bed; Fig. 3; elementary sequence 21), the data obtained reveal an almost constant palaeotransport direction towards the north throughout the section (Fig. 3).

At some levels, the cross-bedded grain- and packstones form packages, 4 to over 8 m thick (Fig. 3; elementary sequences 31–34). According to Tronkov (1968), such sediment bodies form regionally traceable bed packages, representing stratigraphic marker horizons. The availability of appropriate outcrops in the studied area allows lateral tracing of one distinct bed, the so-called Zitolub Bed. Its thickness can vary over a relatively short distance (less than 500 m) from more than 4 to less than 2 m. However, all measurements of palaeotransport direction show the same predominant orientation.

Soft-sediment deformation structures are rare and mainly connected with packstone beds. They were observed only in isolated cases as load casts (Fig. 3; base of

---

Fig. 5. Microphotographs of mud- and wackestones (for position of samples see Fig. 3; HSd: highstand deposits; TSd transgressive deposits; all scale-bars represent 0.5 mm). **A.** Bioclastic wackestone with fringes of calcite cement around bivalve shells (early HSd of elementary sequence 1). **B.** Bioclastic wackestone, gastropod shell partly filled with micrite, partly with clear calcite spar or with dolomite crystals (TSd of elementary sequence 5; early HSd of small-scale sequence 1; TSd of the first medium-scale sequence). **C.** Bioclastic wackestone, originally aragonitic gastropod shell dissolved after having been filled with carbonate mud and small peloids (middle TSd of elementary sequence 7; maximum-flooding zone of the first medium-scale sequence). **D.** Bioclastic wackestone with thick recrystallized bivalve shells (early HSd of elementary sequence 8; maximum-flooding zone of the first medium-scale sequence). **E.** Bioclastic wackestone with thick bivalve shells and echinoderm fragments highlighted by arrows (HSd of elementary sequence 12; early HSd of the first medium-scale sequence). **F.** Silty mudstone with dark, clay- and organic-rich wavy layers that create lamination (HSd of elementary sequence 4; maximum-flooding zone of small-scale sequence 1). **G.** Dolo-mudstone (late HSd of elementary sequence 7; early HSd of small-scale sequence 2; maximum-flooding zone of the first medium-scale sequence). **H.** Bioclastic dolo-wacke-packstone with echinoderm fragments highlighted by arrows, note thin fringe of syntaxial cement (early HSd of elementary sequence 14; HSd of small-scale sequence 2; early HSd of the first medium-scale sequence).

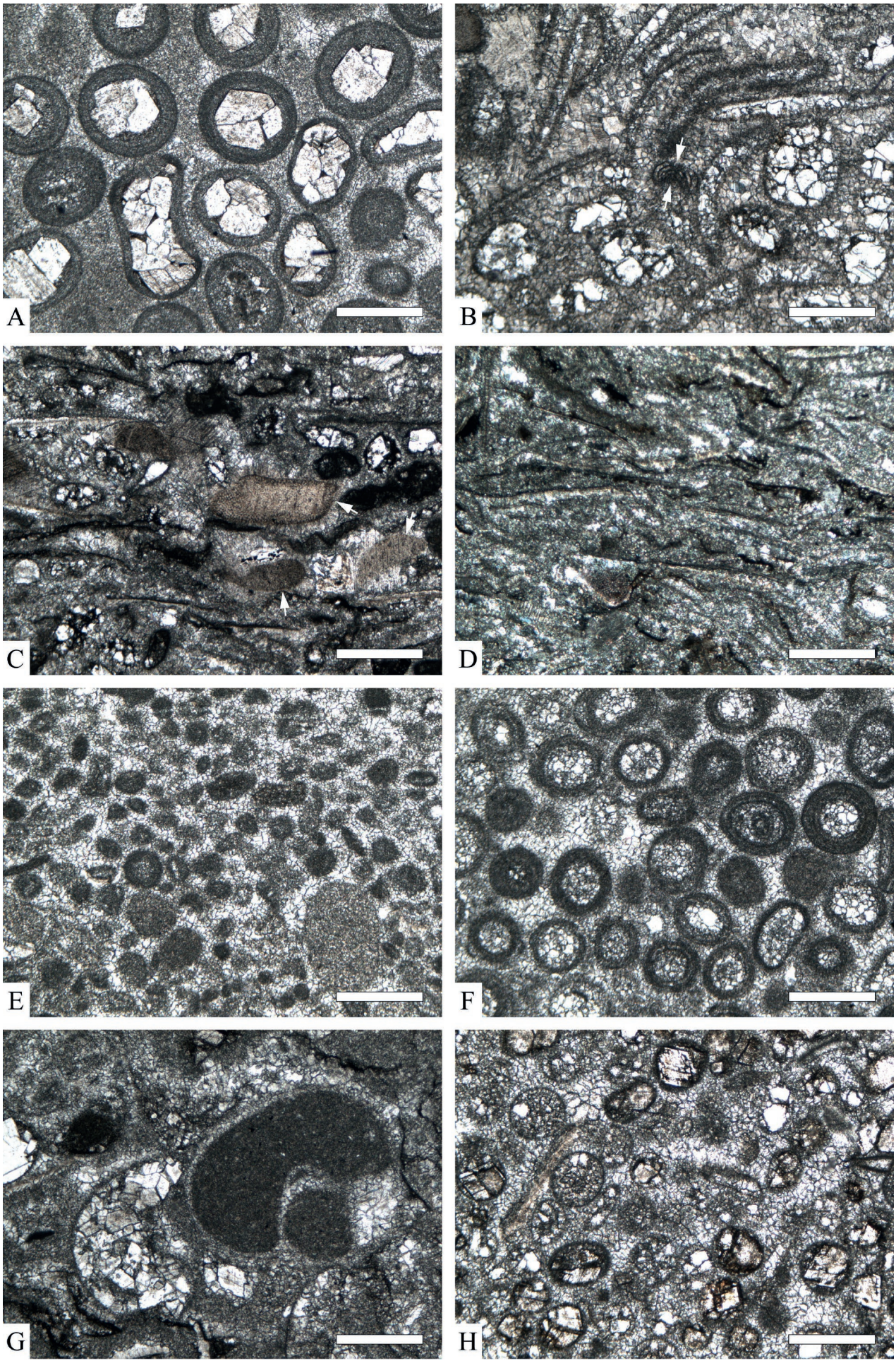
A
B
C
D
E
F
G
H

elementary sequence 39) and folding (Fig. 3; elementary sequence 35).

The variety of morphology, scale, and orientation of cross-bedding observed in grain- and packstones, the accretion and reactivation surfaces, and the intercalation of these features indicate highly variable high-energy settings. The presence of intraclasts, some of them semi-lithified, imply an almost permanent subaqueous erosion by waves and currents. Wavy bedding and the variable orientation of the cross-beds indicate a tidal influence (e.g., Reineck and Singh, 1975; Gonzales and Eberli, 1997).

Dolostones

Most of the dolomites are wacke- and mudstones (Fig. 5G), with only few dolomitized grain- and packstones (Fig. 5H) and clayey and marly dolostones. They predominate in the upper part of the studied section, above the Sfrazen Bed, where they form an 8.1-m-thick package of dolo-wacke- and packstones (Fig. 3; elementary sequences 63–65), intercalated with several claystones and marls, 10–15 cm thick.

Generally, dolomites form medium to thin (5–30 cm), rarely thick (almost 1 m, Fig. 3; elementary sequence 20) beds with massive, laminated, or nodular structure. The lamination is mm- to cm-scale, often wavy. In the packstones, dolomitization may affect part of the matrix and/or partially the fragments, selectively replacing some of them, while in the wacke- and mudstones it may affect the whole facies, forming mainly crypto- and microcrystalline rocks. They are also associated with desiccation cracks (Fig. 3; elementary sequences 5 and 43), tepees and flat pebbles that form local lags (Figs 3, 7E; elementary sequences 43 and 50). In particular cases, most often as part of the filling of small-scale channels, they form local lenses (Figs 3, 4J; elementary sequences 12, 54, and 61).

The dolomitized mud- and wackestones contain mainly peloids, ostracods and benthic foraminifera, while in the grain- and packstones, bioclasts and ooids are present (Fig. 5H). In a dolo-mudstone bed, just below a level with tepees and flat-pebble lags, a fenestral fabric with gypsum was observed (Fig. 7A). Dome-shaped stromatolites, developed in thick-bedded mud- to wackestone, were documented (Fig. 7B). As in the fine-grained limestones, in some dolo-wackestones thin (1–2 cm) beds of packstone tempestites are found (Fig. 7F). Their erosional base cuts the dolostone lamination.

Synsedimentary, soft-sediment deformation structures occur in slide-connected folding of different scales (Figs 3, 7C; elementary sequences 2, 21, 29, and 54), and in some cases their amplitude can reach 50 cm (Fig. 3; top of elementary sequence 20).

The dolomitic intervals are interpreted as the shallowest, high-salinity sedimentary environment with desiccation cracks and tepee structures marking episodes of subaerial exposure. Moreover, semi-arid climatic conditions were favourable for the microbially-mediated dolomitizaton of microbial mats in a tidal-flat environment (e.g., Petrash *et al.*, 2017) and/or early-diagenetic reflux dolomitization (e.g., Adams *et al.*, 2018). Strata-bound dolomitization and the association with features indicating peritidal conditions, suggest penecontemporaneous processes, though late-diagenetic dolomitization cannot be entirely ruled out (e.g., Lukoczki *et al.*, 2019). Multiple storm events and/or strong tidal currents ripped up cohesive sediment, firmgrounds, and microbial mats to form flat-pebble conglomerates and lag deposits (e.g., Hardie and Ginsburg, 1977; Hillgärtner *et al.*, 2002). In the case of the grainstones, the dolomitization took place during early diagenesis in the shallow burial zone (Fig. 3, elementary sequences 1 and 61).

Marls, silt- and claystones

Rocks with terrigenous components such as marls, silt- and claystones are minor lithologies of the section studied. They are cm- to dm-bedded, laminated, and rarely massive. They mostly occur in the lower part of the section, with the thickest interval of over 10 m (Fig. 3; elementary sequences 22 and 23) characterized by intercalation with dolo-wacke- and mudstones. This interval also reveals tepees and desiccation cracks (Fig. 7D) and shows numerous, syndepositionally folded, fine-grained beds. Convolute structures also were recognized in several thin (4–7 cm) marl and claystone beds in the lower part of the section. In contrast to the structures associated with subaerially exposed environments, these latter structures formed in a subtidal environment.

Another level with soft-sedimentary deformation within such rocks is the base of the Sfrazen Bed, where dolo-marls intrude into the overlaying thick, cross-bedded grainstones, forming flame structures (Fig. 9E).

Erosion and shear surfaces

Erosional surfaces are common features of the section studied. The erosional amplitude generally varies between 5 and 15 cm, but in places reaches several tens of centimetres

---

Fig. 6. Microphotographs of grain- and packstones (for position of samples see Fig. 3; HSd: highstand deposits; TSd transgressive deposits; all scale-bars represent 0.5 mm). **A.** Ooidal grainstone, ooid cores replaced by coarse dolomite crystals (base of TSd, elementary sequence 1). **B.** Bioclastic grain-packstone with forams (arrows), bivalve shells and ooids replaced by calcite spar, only the thin micritic envelopes are preserved (base of TSd, elementary sequence 2). **C.** Bioclastic grainstone with echinoderm fragments highlighted by arrows (elementary sequence 12; early HSd of the first medium-scale sequence). **D.** Bioclastic packstone rich in thin bivalve shells (base of TSd, elementary sequence 8; early HSd of small-scale sequence 2; maximum-flooding zone of the first medium-scale sequence). **E.** Peloidal grainstone (base of TSd, elementary sequence 21; early TSd of small-scale sequence 5; base of the Zitolub Bed). **F.** Ooidal grainstone, ooid cores replaced by calcite spar (middle TSd, elementary sequence 21; base of the Zitolub Bed). **G.** Bioclastic grain-packstone with gastropods (elementary sequence 25; early HSd of the second medium-scale sequence). **H.** Bioclastic and ooidal grainstone, ooid cores replaced by calcite or dolomite (TSd, elementary sequence 26; early TSd of small-scale sequence 6).

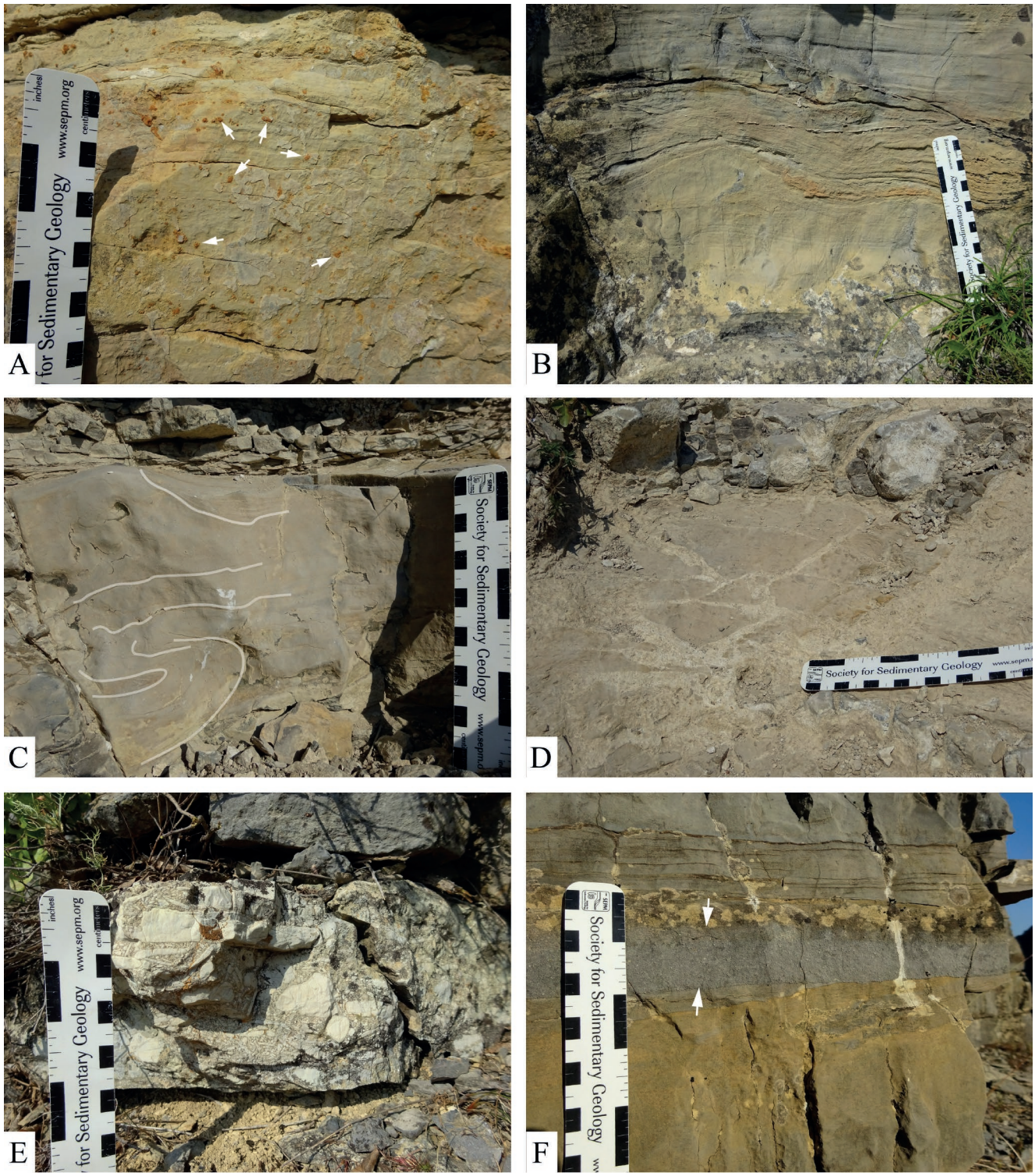

Fig. 7. Dolomite lithologies. **A.** Wavy-laminated dolo-mudstone with fenestral fabric with gypsum highlighted by arrows (elementary sequence 42). **B.** Dome-shaped dolomitized stromatolite developed in the uppermost part of the fourth small-scale sequence (elementary sequence 20). **C.** Small-scale slump-generated deformation (outlined) in dolo-mudstone bed from the uppermost part of elementary sequence 21. **D.** Plane view of desiccation cracks with angular lithoclasts in dolo-marls (elementary sequence 22). **E.** Clast-supported lag deposit composed of platy, subrounded, poorly sorted pebble-sized dolomite intraclasts (elementary sequence 43). **F.** Thin tempestite bed of packstone (between arrows) with normal graded bedding and erosional base in laminated dolo-wackestone from the lower part of elementary sequence 10. The numbering of the elementary sequences is as in Figure 3.

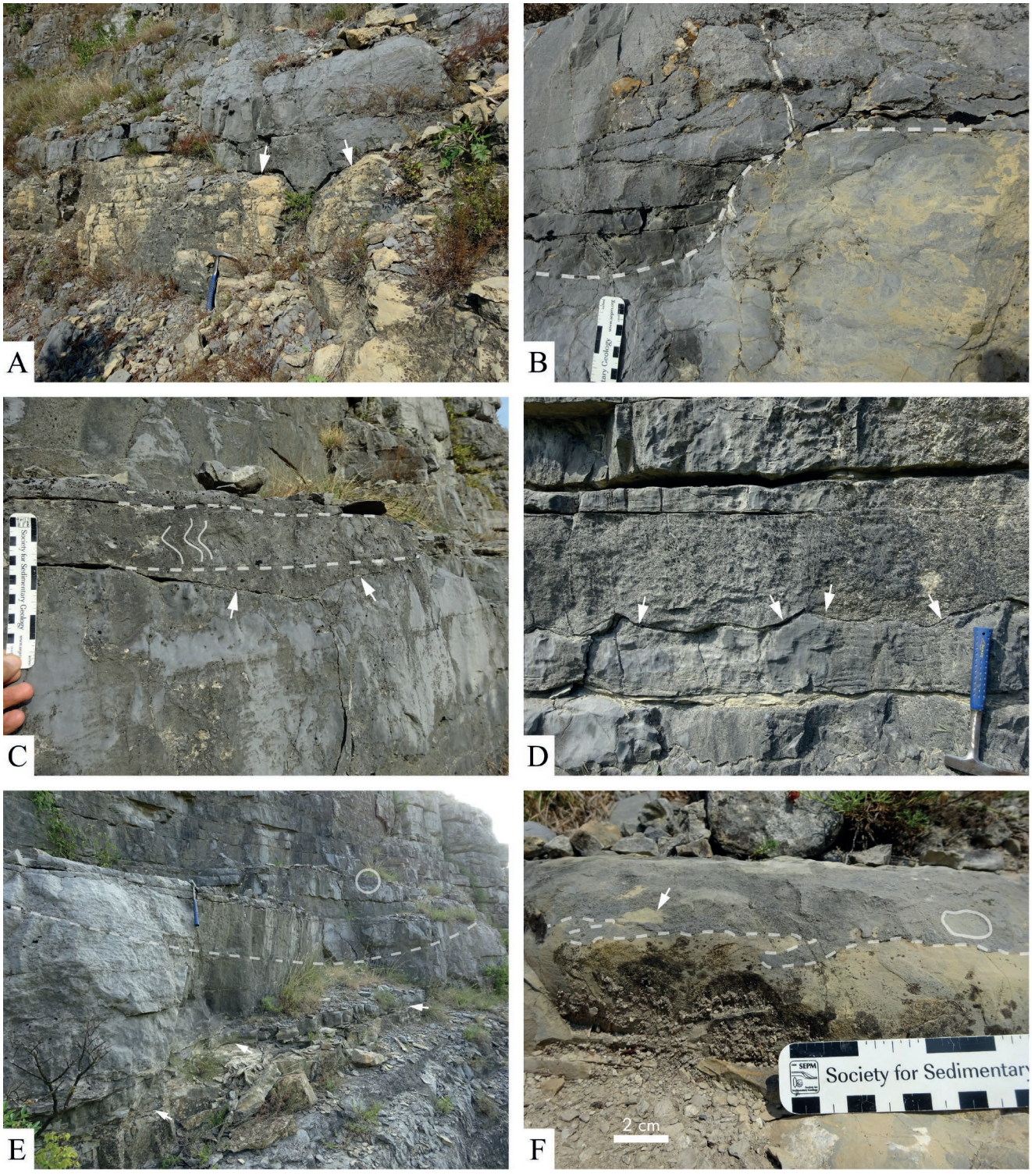

Fig. 8. Erosional and slide/slump generated surfaces. **A.** 40 cm deep steep-sided erosional surface (below arrows) on top of dolo-wackestone, overlain by cross-bedded packstone from the limestone that marks the transgressive surface in the lower part of elementary sequence 54. **B.** Steep flank (dashed line) of channel at the base of elementary sequence 61, filled with alternation of thin beds and lenses of wacke- and packstones and cross-bedded grainstones. The channel is developed in bioturbated dolo-mudstones. **C.** Low-amplitude erosional surface (arrows) developed in weakly bioturbated mud- to wackestones and overlain by packstones with sigmoidal syndepositional soft-sediment deformation (between dashed lines). Laterally, over a very short distance, the soft-sediment deformation corresponds to a level with small-scale sliding structures at the maximum-flooding surface of elementary sequence 6. **D.** Low-amplitude (8 cm) wavy, probably storm-generated erosional surface (arrows) in mudstones, overlain by massive wackestones. Hammer handle for scale, elementary sequence 6. **E.** 65 cm-deep channel-like surface (dashed line), connected with a local slide in wackestones from the transgressive part of elementary sequence 6. Arrows mark the elementary sequence boundary, circle the erosional surface from C. Hammer for scale. **F.** Firmground surface (dashed line) at the top of dolo-wackestone, overlain by packstones with solitary dolostone (below the arrow) and limestone (outlined) intraclasts (elementary sequence 21). The numbering of the elementary sequences is as in Figure 3.

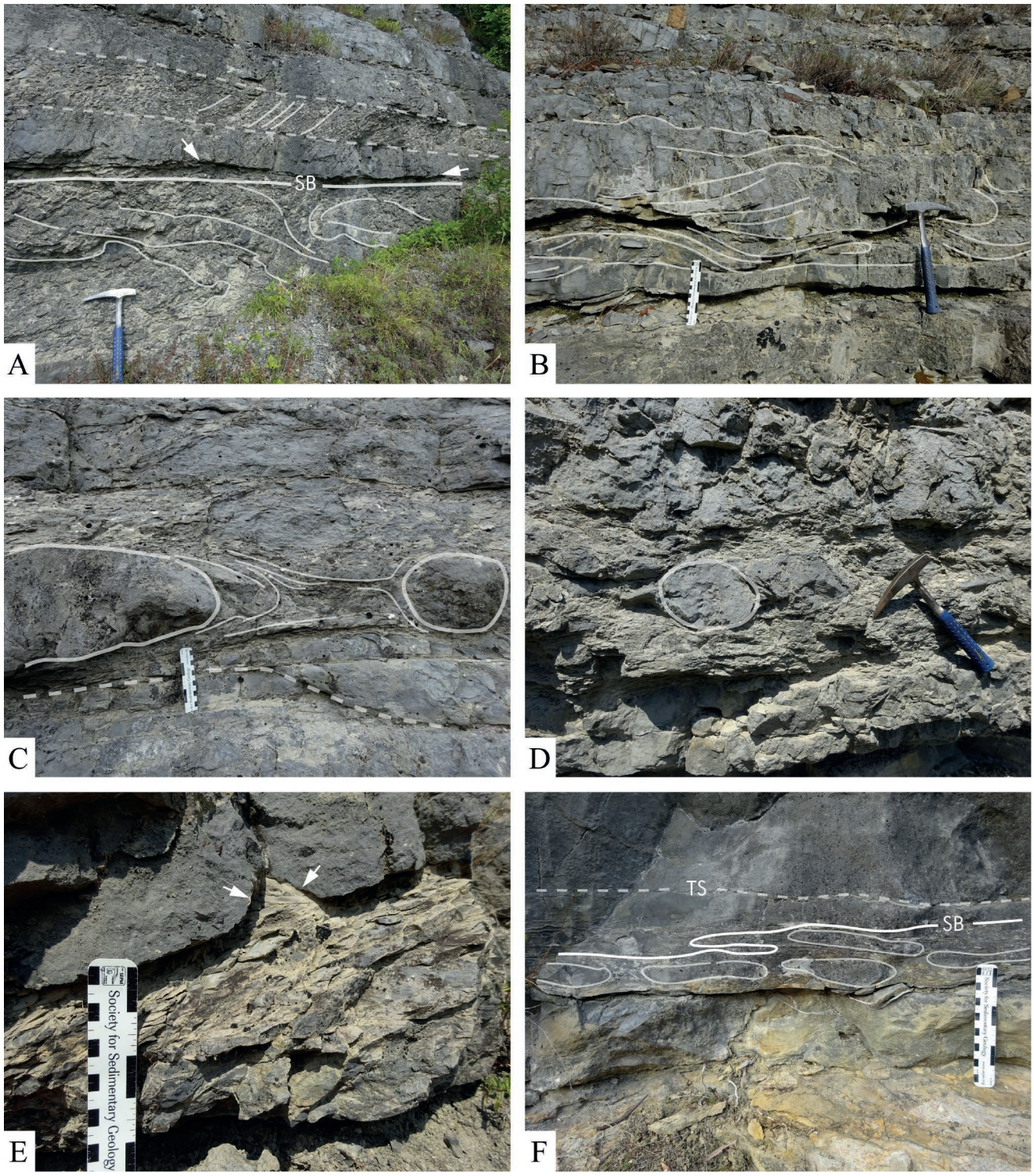

Fig. 9. Syndepositional deformation structures. **A.** Large-scale slump-generated deformation (outlined) in mud- to wackestone from the uppermost part of elementary sequence 29. Above another thinner bed with the same lithology and steeply dipping subparallel shear surfaces (between dashed lines), lower part of elementary sequence 30. The boundary between the elementary sequences (SB) and the transgressive surface (arrows) is marked. Hammer for scale. **B.** View oblique to the slumping direction of deformed package (outlined) of marl and wackestone of the maximum-flooding zone; elementary sequence 4. Hammer for scale. **C.** Ball-and-pillow structure of packstone (outlined) in clayey wackestone, resulting from the development of the stepped sliding surface (dashed line), elementary sequence 8. **D.** Concentric ball-and-pillow structure (outlined) as part of large-scale slump in the upper part of elementary sequence 6. Hammer for scale. **E.** Dolo-marls with flame structure (arrows) in the uppermost part of elementary sequence 31, intruding into cross-bedded grainstone from the base of the Sfrazen Bed. **F.** Ball-and-pillow structure of wackestone in clayey dolo-mudstone developed at the top (deformed sequence boundary SB) of elementary sequence 6. **G.** Laterally well traceable (over 200 to 250 m) sigmoidal structure (highlighted

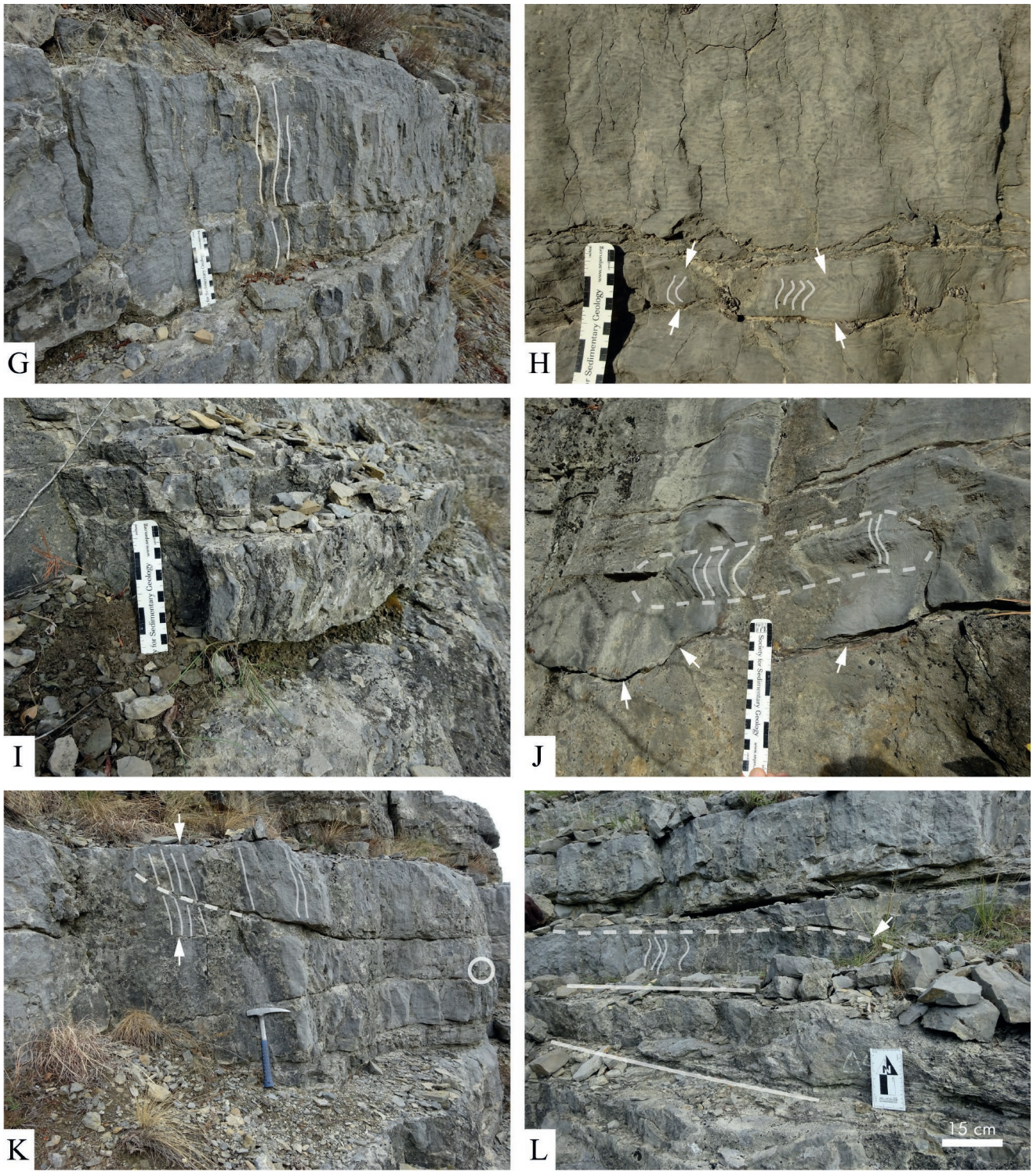

by vertical white lines) comprising the top 40 cm of the wacke-mudstones in the uppermost part of elementary sequence 9. **H.** Locally (several decimetres) developed sigmoidal structure (between arrows), situated 35 cm below G. Above, a wavy structure is recognized. **I.** Vertical sigmoidal structure that laterally correlates with a slump shear surface in the upper part of elementary sequence 8. **J.** Small erosional channel (above arrows), developed in transgressive packstone from the base of the first elementary sequence. In the right flank of the channel fill a laterally restricted (about 30 cm) sigmoidal structure (between dashed lines) is visible. **K.** Lateral view of the level of G with the large-scale sigmoidal structure (between white arrows) and inclined shear surface (dashed line). The circle marks the level of the structure shown in H. Hammer for scale, elementary sequence 9. **L.** Wackestone beds from the upper part of elementary sequence 6 with folded (between full lines) and sigmoidal (dashed line marks the top) structures. The top of the sigmoidal structure abruptly decreases to the right and finally disappears (arrow). The numbering of the elementary sequences is as in Figure 3.

(Fig. 3; elementary sequences 54 and 61) and even up to 80 cm (Fig. 8A). The majority of channel-like erosion surfaces show gently inclined flanks (Fig. 8C), but in some cases they are stepped (Fig. 8A) or very steep to almost vertical (Fig. 8B), indicating a relatively advanced degree of cohesion and early lithification of the sediment, into which the channel was cut (Ajdanlijsky *et al.*, 2019).

Based on their lateral traceability, two groups are distinguished: erosional surfaces that can be easily followed over distances of several tens of metres or more and surfaces with laterally restricted development of a few decimetres up to several metres (Figs 8C, 9J). The morphology is irregular (Figs 8D, 9J) or symmetrical and channel-like (Fig. 8A, C).

Stacking of multiple erosional surfaces is documented at several levels, mainly in the upper part of the section (Fig. 3; elementary sequences 54 and 61).

Several specific surface morphologies can be distinguished. A wave-like morphology was observed with pointed, narrow crests and wide and smooth troughs (Figs 3, 8D; elementary sequence 6). The amplitude ranges from 6 to 8 cm. These surfaces mark the top of massive to weakly laminated mudstones, overlain by massive wackestones (Fig. 8D). They can be traced over several tens of metres, where they gradually turn into flat bedding planes. They cut the lamination in the underlying fine-grained rocks and no sign of loading was observed. The origin of these surfaces is not fully understood, but it is hypothesized that they are the result of storm-wave erosion in a shallow lagoon.

Another group of channel-like surfaces have very smooth and sloping contours, developed in intervals within beds or bed sets with fine-grained texture. Their amplitude ranges from 10 to 30 cm (Fig. 9K) to over 65 cm (Fig. 8E). Since there is no change in lithology across such surfaces, they are often difficult to distinguish. They are interpreted as shear surfaces, resulting from soft-sediment sliding events.

Firmgrounds

Two different levels with firmground surface development were documented (Fig. 3; elementary sequences 2 and 21). In both cases they mark the top of wackestones, overlain by packstones (Fig. 8F). The surfaces are irregular, with amplitudes of several centimetres. Scattered small intraclasts were observed along these surfaces, which resulted from reworking of the consolidated sediment.

Syndepositional soft-sediment deformations

Small-scale folding, slumps, load casts, ball-and-pillow structures, as well as sets of sub-vertical, sigmoidal shear surfaces of different scale and morphology were documented in the studied section, mainly in the lower part (Fig. 3). They may occur as single features, closely spaced and of the same type, or as a combination of different types. For example, within an interval 5 to 6 m thick, 5 to 9 separate levels of up to three different types of such syndepositional soft-sediment deformation structures were observed (Fig. 3; elementary sequences 6, 8–9, and 29–30). At the same time, up to four soft-sediment deformation levels, similar in scale, were established above each other within 3.5 m (Fig. 3; elementary sequence 28). In lateral distribution, they are both local, developed within a few tens of centimetres to several metres, or traceable over tens and even hundreds of metres.

Slump structures are present at 14 distinct levels (Fig. 3). Generally, these slumps are characterized by chaotic folding, most commonly affecting 25–40 cm thick intervals (Fig. 9B), in some cases exceeding 70 cm (Fig. 9A). Usually, each slump is developed at one distinct level, but they can also be part of cascading sets above a basal shear surface (Fig. 8E). Ball-and-pillow structures are often associated with such cascading slump structures, additionally deforming the hosting materials (Fig. 9C). In particular cases, the ball bodies have a concentric inner structure (Fig. 9D). Simple and pendulous load casts (Figs 4L, 9F) can also be associated with small-scale ball-and-pillow structures.

Small-scale folding is another type of syndepositional soft-sediment deformation, common in wacke- and mudstones, observed in almost the entire section studied (Figs 3, 7C).

Other commonly observed features in wacke- and mudstones are intervals with a set of sub-vertical shear surfaces, often with sigmoidal geometry. Their thickness ranges between 5 to 15 cm (Fig. 9H, I, J, L), but in some beds may reach or even exceed 40 cm (Fig. 9A, G). Generally, they are locally developed structures, extending laterally over several tens of centimetres (Fig. 9H, J) or several metres (Figs 8C, 9I, L), and only in very rare cases they can be traced laterally over 80 m (Figs 3, 9G; elementary sequence 9). They are developed above channel floors (Fig. 8C) or in channel flanks (Fig. 9D), laterally corresponding to a local slide shear surface or to a local erosion surface interpreted as storm-induced (Figs 3, 8C; elementary sequence 6). They occur above small-scale folding or slump structures (Figs 3, 9I; elementary sequences 6, 9, 16, and 30). In some places, a direct contact between sigmoidal and slump structures can be observed (Fig. 9L).

The upper bounding surface of the intervals with sigmoidal structures can be flat over some distance, but in many cases it is slightly concave-up or inclined. The reason for the latter is that their amplitude gradually decreases when traced over some distance, and finally the structure disappears laterally (Fig. 9L). The orientation measurements reveal a prevailing NNE–SSW direction of the sigmoidal structures, which are interpreted as having formed by sliding of soft but cohesive sediment, possibly by instabilities at channel margins (Hardie and Garrett, 1977). Another factor that could have controlled the development of such syndepositional soft-sediment deformation structures is the seafloor morphology. A combination of rapid sedimentation and a suitable slope, together with triggering factors, such as storm waves, could have led to the slumping and sliding of soft sediment. There are no clear indicators of seismic activity in the area and the limited lateral extension of these features makes an interpretation as seismites unlikely (Montenat *et al.*, 2007).

The observed differences in scale of soft-sediment folding, slumps, ball-and-pillow structures and the sets of sub-vertical, sigmoidal shear surfaces evidence syndeposi-

tional deformation processes in subtidal ramp settings. Small-scale deformation structures, occurring in intertidal to supratidal environments, are probably related to expansion (forming tepees) and retraction (forming desiccation cracks) of the soft but cohesive sediment.

SEQUENCE STRATIGRAPHY AND CYCLOSTRATIGRAPHY

The sequence- and cyclostratigraphic interpretation follows the concepts proposed by Strasser *et al.* (1999). The sequence-stratigraphic nomenclature is that of Catuneanu *et al.* (2009), applied independently of the scale of the sequences (Posamentier *et al.*, 1992; Catuneanu, 2019). Elementary sequences are the smallest units, in which facies trends and sedimentary structures indicate a cycle of sea-level change (first deepening, then shallowing). Because even these metre-scale units can be interpreted in terms of sequence stratigraphy, the present authors prefer to call them "sequences" and not "cycles". Small-scale sequences are composed of several elementary sequences and generally display first a deepening and then a shallowing trend, with the shallowest facies at the boundaries. Several small-scale sequences compose a medium-scale sequence, which again displays a general deepening-shallowing trend of facies evolution with the relatively shallowest facies at its boundaries. If several elementary sequences make up an interval of shallowest or deepest facies, a sequence-boundary zone and a maximum-flooding zone, respectively, is defined (Montañez and Osleger, 1993).

A total of 67 elementary sequences was identified in the Opletnya Member of the section studied (Fig. 3). These are generally grouped in fives to form 14 small-scale sequences, the last one incompletely recorded as a result of erosion at the top of the Mogila Formation (Fig. 3G). Two or four small-scale sequences are bundled into 5 medium-scale sequences, in which three parts can be recognized: transgressive, maximum-flooding, and highstand deposits.

Elementary sequences

The elementary sequences are defined by their bounding surfaces, composition, facies trends, and sedimentary structures that indicate a cycle of sea-level change. The base of each elementary sequence is marked by the shallowest facies, and/or by a laterally traceable erosional surface (sequence boundary: SB). Elementary sequences can be subdivided into three parts – a lower part that represents the deepening-up transgressive stage (transgressive deposits: TSd), a middle part containing the maximum-flooding surface (MFS) and an upper part representing the shallowing-up highstand stage (highstand deposits: HSd). The facies composition and thickness of these parts varies depending on the position of the elementary sequence within the small-scale and especially within the medium-scale sequence it belongs to (Strasser *et al.*, 1999).

The sequence boundary can be marked by an abrupt facies change, by an erosional surface, by desiccation cracks, or by load casts (implying rapid sediment accumulation over a soft sediment surface). The erosional amplitude commonly is in the range of a few centimetres. Only in one case (Fig. 3; elementary sequence 54) an erosion depth of about 80 cm was measured (Fig. 8A). Above the sequence boundary, well pronounced erosional surfaces may also occur. They are interpreted as transgressive ravinement surfaces (TS), and the sediment between SB and the erosive TS therefore qualifies as lowstand deposit (e.g., Fig. 3, elementary sequence 54). Intraclast lags at the base of elementary sequences are common. Some of them are with diffusive contours, indicating very fast reworking of not well lithified sediments during transgression; SB and TS thus are amalgamated (Fig. 3; elementary sequences 16, 21, 61). Massive, mainly in the lower part of the section (Fig. 4H), and cross-bedded (Fig. 4I) ooidal, peloidal and/or bioclastic pack- and grainstones (Fig. 6A, B, D, G) in the upper part, represent shallow bars or shoals that formed during transgression. In the lower part of the section they form only 6 to 11% of the sequences (Fig. 3; elementary sequences 4 and 6), while in other parts they completely build elementary sequences (Fig. 3; elementary sequences 31–34). In such cases, the base is marked by a transgressive surface and the sequence boundaries generally are not developed (elementary sequences defined by transgressive surfaces; Strasser *et al.*, 1999). The sequence boundary also can be associated with load cast and flame structures (Fig. 9E, F). In the upper part of the section, in some units, local small-scale erosional channel stacking is observed (Fig. 3; elementary sequences 54 and 61). Thin tempestite beds are also documented (Fig. 4F).

The maximum-flooding surface marks the top of the transgressive beds or can be identified by the relatively deepest facies and/or intense bioturbation (Fig. 4E, K) and, in many cases, syndepositional soft-sediment deformation such as small-scale folding. Firmgrounds are recorded (Fig. 3; elementary sequence 8). Along and above this level, the amount of terrigenous components increases, forming beds of marls or of mixed siliciclastic-carbonate sediment.

In the early highstand part of these elementary sequences, massive and laminated (Fig. 4A) and nodular, often bioturbated wacke- and mudstones predominate (Fig. 5A, D, E). In the lower part of the section, these intervals are dominated by laminated lime- and clayey mud- and wackestones (Fig. 3; elementary sequences 7 and 8), or by irregular intercalation of marls, limy claystones and mudstones (Fig. 3; elementary sequences 22 and 23). Slide shear surfaces (Fig. 9C, K) and different types of small-scale syndepositional folded beds (Figs 7C, 9A, B, L) were recorded. Sigmoidal structures of different scales are very common (Figs 3, 9G, H, I, K, L; elementary sequences 5, 6, 9, 16, and 30). In the late highstand part desiccation cracks (Fig. 7D), stromatolitic beds, and – rarely – evaporites also were observed (Fig. 7A, B). In the upper part of the section, the highstand intervals of the elementary sequences are dominated by nodular mud- and wackestones. If developed, the content of dolomite (Fig. 5G, H) or partially dolomitized limestones (Fig. 8B) and dolo-marl beds gradually increases towards the top and in the uppermost part of the section almost all of the elementary sequences

are made up of dolomitic limestone (Fig. 3; elementary sequences 64 and 65).

Within the lower part of the section, local, small-scale erosional channels (Fig. 3; elementary sequences 7 and 15) and slide shear surfaces (Fig. 3; elementary sequences 2 and 5), associated with syndepositional soft-sediment deformations, are developed as small-scale folding and slump structures. This stage is also associated with some storm-wave-induced erosion (Fig. 8D).

Small-scale sequences

The elementary sequences described, grouped into sets of five, form a succession of 14 small-scale sequences (Fig. 3). Mainly in the lower part of the section and only in particular cases in the upper part, their base is marked by a pronounced erosional surface (Fig. 8B) and/or a intraclast lag (Fig. 4G). Ball-and-pillow structures are also developed (Fig. 9F). The measured erosional amplitude of these surfaces ranges from a few centimetres to decimetres (Fig. 8B). Stacking of several erosional surfaces within one elementary sequence, situated at the base of the small-scale sequences, is recorded in one case (Fig. 3; small-scale sequence 13). In some cases, the base is not defined by an erosional surface but interpreted with reference to lithological changes and by the stacking pattern of the elementary sequences (Fig. 3; small-scale sequences 8–10).

Generally, small-scale sequences show first a deepening then a shallowing trend and their boundaries exhibit the shallowest facies. Generally, their lower, early transgressive part is dominated by limestones, i.e., litho- and bioclastic or ooid-dominated pack- and/or grainstones (Figs 4G, 6A, E, H). Massive, laminated, planar, and trough cross-bedding with intraclasts is common (Fig. 4I). Locally restricted small-scale erosional channels, reactivation surfaces and lateral accretion surfaces were documented (Fig. 4J). Different types of small-scale cross-bedding, indicating wave or current hydrodynamic regimes, are also typical for this part. The cross-bedding can be associated with partially dolomitized limestones (Fig. 4J). Most often the palaeotransport directions vary in a wide range of orientation (Fig. 3; small-scale sequence 5, 7); however, unidirectional patterns also occur (Fig. 3; small-scale sequences 8, 13).

Upsection, marking a deepening facies trend, the proportion of pack- and grainstones in the small-scale sequences decreases and the proportion of wackestone, often nodular or laminated, increases. Bioturbation also increases (Fig. 4K) and thin shell beds are common features (Fig. 4D). The erosion is local and small in scale (Fig. 3; elementary sequences 2, 3, and 7), reworking processes are often related to slide shear surfaces and slump structures (Figs 3, 8E; elementary sequences 2 and 6), and firmground surfaces were recorded (Fig. 8F). Intervals with tempestites (Fig. 4F) and storm-wave-induced erosion (Fig. 8D) were observed. These features indicate shallow depositional environments with, mainly in the lower part of the section, local or even laterally developed instability of the still soft sediments, leading to syndepositional deformation (Fig. 9D). Ball-and-pillow structures, indicating a relatively fast rate of sedimentation, also were observed (Fig. 4L).

The turn-around to a shallowing facies trend was associated with a gradual increase of the amount of terrigenous material (Fig. 5F), penecontemporaneous or early-diagenetic dolomitization, and syndepositional soft-sediment deformations. The intensity of bioturbation in the interval of maximum flooding is still high and gradually decreases upwards (Fig. 4B, E). The higher terrigenous content led to more nodular structures and platy bedding (Fig. 4C), well represented in the lower part of the section (Fig. 3; small-scale sequences 2, 3, and 5).

In other cases, the shallowing-upwards trend is associated with an increase in packstone beds (Fig. 6D), often cross-bedded, dolomitized limestones and dolomites (Fig. 5G, H). These can be associated with different types of lag deposits, tepees, and desiccation cracks (Figs 3, 4H, 7D; elementary sequences 5, 20, 29, 43, 54–55). Within dolomitic intervals, levels of stromatolites (Fig. 7B) and tempestite beds (Fig. 7F) were observed. In places, the dolomitization is restricted to a local channel (Fig. 8A).

Other highstand features of small-scale sequences are the increase of erosional and syndepositional soft-sediment deformation structures, especially in the lower part of the section, where sigmoidal structures are common and intercalate or even superimpose small-scale folding, ball-and-pillow and slump structures (Fig. 9A–C, G–I, K). Commonly, their development is associated with slide shear surfaces of different scales (Fig. 8E).

Variations from the above described pattern were observed in two cases: in the Sfrazen Bed (Fig. 3; small-scale sequences 7 and 8), where bioclastic to intraclastic packstones predominate almost entirely, and in the uppermost part of the section (Fig. 3; small-scale sequences 13), where dolomitic lithology is more widely represented.

The thickness of the small-scale sequences varies between 6.7 and 29.8 m (average 12.9 m). Below the Sfrazen Bed, their thickness is constantly over 15.5 m, while above the Sfrazen Bed, it ranges between 6.5 to 10 m (Fig. 3).

Medium-scale sequences

Five medium-scale sequences have been identified, each subdivided into three parts – transgressive, maximum-flooding and highstand deposits. The number of small-scale sequences within them, however, is not equal and varies from two to four (Fig. 3). The base of the first medium-scale sequence corresponds to the base of the Mogila Formation that marks the termination of a significant terrigenous supply to the basin and the beginning of shallow-marine sedimentation in the study area. This is the second early Anisian regional transgression, after the first one at the base of the Svidol Formation (Ajdanlijsky *et al.*, 2019).

The medium-scale sequences are defined by particularly well-developed sequence boundaries and by the trend of stacking of the small-scale and elementary sequences, which display a general deepening-shallowing trend.

In the transgressive part of a medium-scale sequence, the sequence boundary (SB) and transgressive surface (TS) of the elementary sequences are very close to each other or even amalgamated. The average thickness of the elementary sequences from the transgressive part of the medium-scale

sequences is 2.3 m. The thickest elementary sequences – elementary sequences 7 (5.2 m) and 21 (7.3 m) – occur in the two lower, medium-scale sequences (Fig. 3). The lower part of elementary sequence 21 is the Zitolub Bed, which has a varying thickness. Over a relatively short distance of about 400 m, a decrease from 3.6 to 1.9 m was observed. Regarding the vertical thickness trends of elementary sequences in the medium-scale sequences, the first and fourth medium-scale sequence document a gradual upwards thickening, while the third one shows upwards thinning. Another feature of the section studied is that in its lower part, the average thickness of elementary sequences is in the range of 3.5 to 4 m, while in its upper part, above the Sfrazen Bed, it is in the range of 1.5 to 1.6 m.

Wacke- and mudstones (Fig. 5C, D) dominate the elementary sequences in the maximum-flooding to early highstand stages of the medium-scale sequences (Fig. 3). In these intervals, packstones (Fig. 6D) are rare and completely absent in the lower part of the section. Thin grainstone beds at the base of elementary sequences were documented mainly in the uppermost parts of the section. The sequence boundaries are erosional or defined as a sharp lithological contact (Fig. 3; elementary sequences 23, 40, and 41). In places, load cast structures were observed (Fig. 3; elementary sequence 9). The transgressive surface of these elementary sequences often is not recognizable, but its position probably is close to the sequence boundary. The transgressive part of the elementary sequences found in the maximum-flooding to early highstand intervals of the medium-scale sequences is dominated by laminated to massive wacke- and mudstones that intercalate with thin beds of clayey mudstone and marls containing echinoderm fragments (Fig. 5E).

In some medium-scale sequences, the maximum-flooding and early highstand stages are marked by a significant increase of the terrigenous component (Fig. 3; elementary sequences 12 and 22–23). In the lower part of the section, the same parts of the sequences are also characterised by relatively intensive syndepositional soft-sediment deformations (Figs 3, 9A, C, F–I, K; elementary sequences 12–19 and 26–30).

In the highstand stages of the medium-scale sequences, the base of the elementary sequences generally is developed as packstones and grainstones (Figs 3, 4H, 6C, G). However, in the lower part of the section, these lithologies are rare (Fig. 3; elementary sequences 12–19), while in the upper part they increase and can form almost the entire transgressive part of the sequences (Fig. 3; elementary sequence 44–48). Massive and laminated wacke- and mudstones, occasionally intercalated with mixed siliciclastic-carbonate or even claystone beds, are developed in this upper part. In the uppermost part of the section, dolomite and dolomitic limestones are observed (Fig. 3; elementary sequences 64 and 65). Elementary sequence boundaries in the highstand intervals of the medium-scale sequences are more often developed as erosional surfaces, and desiccation cracks and tepee structures were observed (Figs 3, 7E; elementary sequence 50). Intraclast lags and imbrication structures also were recorded.

Regarding the thickness ranges of the elementary sequences in the highstand stages of the medium-scale sequences, a similar pattern as documented in the transgressive stages was observed. Their average thickness is around 2.8 m, and the thickness of the elementary sequences in the lower two medium-scale sequences is more than twice (3.3 to 4.0 m) that above the Sfrazen Bed (1.3 to 1.8 m). The thickest units were documented in the lower parts with 7.0 m (elementary sequence 20) and 6.4 m (elementary sequence 25). An upwards-thinning trend of the elementary sequences was observed in almost each of the medium-scale sequences.

Regarding the individual medium-scale sequence thickness, a fairly constant decreasing-upwards trend was observed. The lowermost (first) unit is the thickest (67.5 m) and includes small-scale sequences 1 to 4 (first 20 elementary sequences). The second medium-scale sequence (46.2 m) is composed of small-scale sequences 5 and 6. The thick high-energy deposits in small-scale sequences 7 and 8 form the transgressive part of the third medium-scale sequence. It is difficult to define the top of this medium-scale sequence, but there is evidence for prolonged subaerial exposure and intensive reworking at the top of elementary sequence 50, with small channel stacking, tepees and lag deposits. The thickness of the third medium-scale sequence (34.2 m) is less than, but close to that of the second one. The fourth medium-scale sequence is about 14 m thick and comprises small-scale sequences 11 and 12. The unit is associated with several levels of deep erosion and the prominent erosion surface An1 defining its top (see Discussion). Due to regional, most probably Late Triassic erosion, only 19.8 m of the fifth medium-scale sequence are preserved in the studied Tserovo section.

PALYNOFACIES

The composition of the sedimentary organic matter within elementary sequences was used to complement and underpin the interpretation, based on sedimentological criteria. Changes in terrestrial input, sorting and fragmentation of phytoclasts, and prominent acritarch peaks indicate major flooding and transgressive-regressive phases. In the Tserovo section studied, three major transgressive and three maximum-flooding phases show peak abundances of marine acritarchs (Fig. 2), corresponding with the sedimentological interpretation.

For a high-resolution interpretation, a 7-m-thick interval in the lower Opletnya Member (representing elementary sequences 8 and 9; Fig. 3) was sampled to identify palynofacies patterns used for sequence interpretation (Fig. 10). The basal dolomite bed shows the lowest percentage (3.2%) of plankton, overlain by bioclastic beds with a marked increase in marine particles, including the first foraminiferal test linings in sample 2. Marine plankton shows peak abundance in sample 4 (24.2%) and sample 8 (28.3%), both horizons showing the highest ratios of opaque to translucent (OP/TR) and equidimensional to blade-shaped (ED/BS) phytoclasts. Translucent phytoclasts of different sizes and shapes are common in samples 2, 3 and 7. High percentages of marine plankton and high OP/TR and ED/BS ratios are still characteristic of samples 5 and 9, while samples 6 and 10 show low plankton percentages of 5.8% and 3.6%, respectively. Within the phytoplankton group, acritarchs are

most abundant in samples 2, 4, 5, 7, 8 and 9, while prasinophytes are predominant in samples 5 and 9 and they are the only plankton group present in samples 1, 6 and 10. Foraminiferal test linings are recorded in samples 2, 4, 7 and 8. Bisaccate pollen grains are the dominant group within the terrestrial particles, spores are rare.

The basal grainstones and wacke-packstones (samples 2 and 3) are interpreted as transgressive deposits, showing a high amount of "fresh" translucent phytoclasts with a huge variety in sizes and shapes and a first plankton peak recorded in sample 2, marking the initial transgressive pulse. In contrast, a very low percentage of plankton (prasinophytes) and a high percentage of terrestrial opaque material of sample 1 is characteristic of late highstand deposits. Thus, the sequence boundary is placed at the base of the bioclastic grainstone bed. Its erosional base might indicate that the sequence boundary is directly overlain by the transgressive surface. The level of sample 4 seems to indicate maximum flooding with a prominent plankton peak of acritarchs belonging to the *Micrhystridium* group, the lowest ratio in continental to marine particles, and the highest percentage of equidimensional, opaque phytoclasts. Percentages of marine plankton and equidimensional, opaque phytoclasts are still high in sample 5 but the influx of terrestrial particles is increasing, characteristic of early highstand deposits. Prasinophytes are the only phytoplankton in sample 6 pointing to a restricted shallow depositional environment, most probably lagoonal. This change in the plankton association, together with a high terrestrial influx of blade-shaped and mixed opaque and translucent phytoclasts, is interpreted as indicative of late highstand deposits.

An increase of marine plankton, dominated by acritarchs, plus the presence of foraminiferal test linings in sample 7 point to transgressive deposits. In sample 8, a peak abundance of marine phytoplankton and foraminiferal test linings marks the next phase of maximum flooding. Again, percentages of marine plankton and equidimensional, opaque phytoclasts are still high in sample 9, but the influx of terrestrial particles is increasing, pointing to early highstand deposits. The overlying dolomitic wackestones in sample 10 show numerous large, blade-shaped phytoclasts and a prasinophyte association of *Tasmanites* and *Cymatiosphaera*, lacking acritarchs. They are interpreted as late highstand deposits. The erosional base of the overlying packstone to grainstone marks the boundary of the following elementary sequence.

DISCUSSION

Lateral facies variation

The cyclic pattern described here has been identified also in the neighboring, northern sections Lakatnik and Sfrazen along the Iskar River gorge, representing the type area of the Mogila Formation (Ajdanlijsky *et al.*, 2019), for which, based on biostratigraphic data, a tentative cyclo- and sequence stratigraphic interpretation was presented (Ajdanlijsky *et al.*, 2018, 2019).

Generally, the stacking pattern of the elementary, small- and medium-scale sequences is the same in all three sections and the variations found are related to the facies and thickness of the sequences (examples in Figs 11 and 12). While the thickness of the first two elementary sequences in all three sections is almost equal, upwards, in elementary sequences 3 to 5, the thickness of those of the Tserovo section gradually increases from 1.5 to over 4 times compared to the same elementary sequences of the Lakatnik and Sfrazen sections (Fig. 11). In the northern sections, the portion of grain- and packstone beds in the elementary sequences is much higher, while in the Tserovo section wacke- and mudstones predominate, with a recognizable increase in marls and mixed carbonate-terrigenous component beds. In the Tserovo section, also syndepositional soft-sediment deformations, such as small-scale folding, slumps, and slide shear surfaces are common features. A pronounced lateral facies variation was recognized for the Tenuis Bed, interpreted as a storm-generated bed (Tronkov, 1968, 1983). In the Lakatnik and Sfrazen sections, this bed is a 0.65 to 1.10 m thick, cross-bedded and partially dolomitized grainstone, containing *Beneckeia tenuis*, while at Tserovo, this stratigraphic level is represented by a 0.15-m-thick, massive grainstone without clear evidence of storm influence.

The described facies variation gradually disappears upsection to the level of the Sfrazen Bed and in the upper part of the sections, the elementary, small- and medium-scale sequences show very similar facies. However, some variations persist (Fig. 12). The uppermost elementary sequences of small-scale sequence 12 of the Lakatnik and Sfrazen sections are dominated by dolo-wacke- and dolomudstones with evaporites, showing desiccation cracks, tepee structures and abundant intraclast lags. For the same stratigraphical level in the Tserovo section, the proportion of dolomites decreases and is finally replaced by intensively bioturbated wacke- and mudstones. In all sections, the boundary between small-scale sequences 12 and 13 is a pronounced erosional surface with an amplitude in the range of 0.2 to 0.7 m, associated with abundant and large intraclast lags. In the Tserovo section, above this boundary, stacking of local erosional channels and domination of cross-bedded pack- and grainstones was observed. These features contrast with those observed in both northern sections, where the proportion of coarse-grained limestone decreases upsection. Despite these differences in all three sections, the thickness range of the elementary sequences is the same.

Lateral and vertical evolution of depositional environments

Mud- and wackestones dominate the lower part of the Opletnya Member in the Tserovo section. The first 6 small-scale sequences show a very small amount of pack- and grainstones and a prominent increase in clay content. This can be interpreted as a low-energy, deeper and more distal setting on the ramp, when compared to the northern sections. The thickness of the elementary sequences in Tserovo decreases upsection, marking a loss of accommodation space. Shallow depositional conditions, documented by the deposition of grainstones and dolostones, then occur in all sections across the ramp, above the Sfrazen Bed.

The consistent orientation of the sedimentary palaeotransport direction towards NNE in almost all the sections,

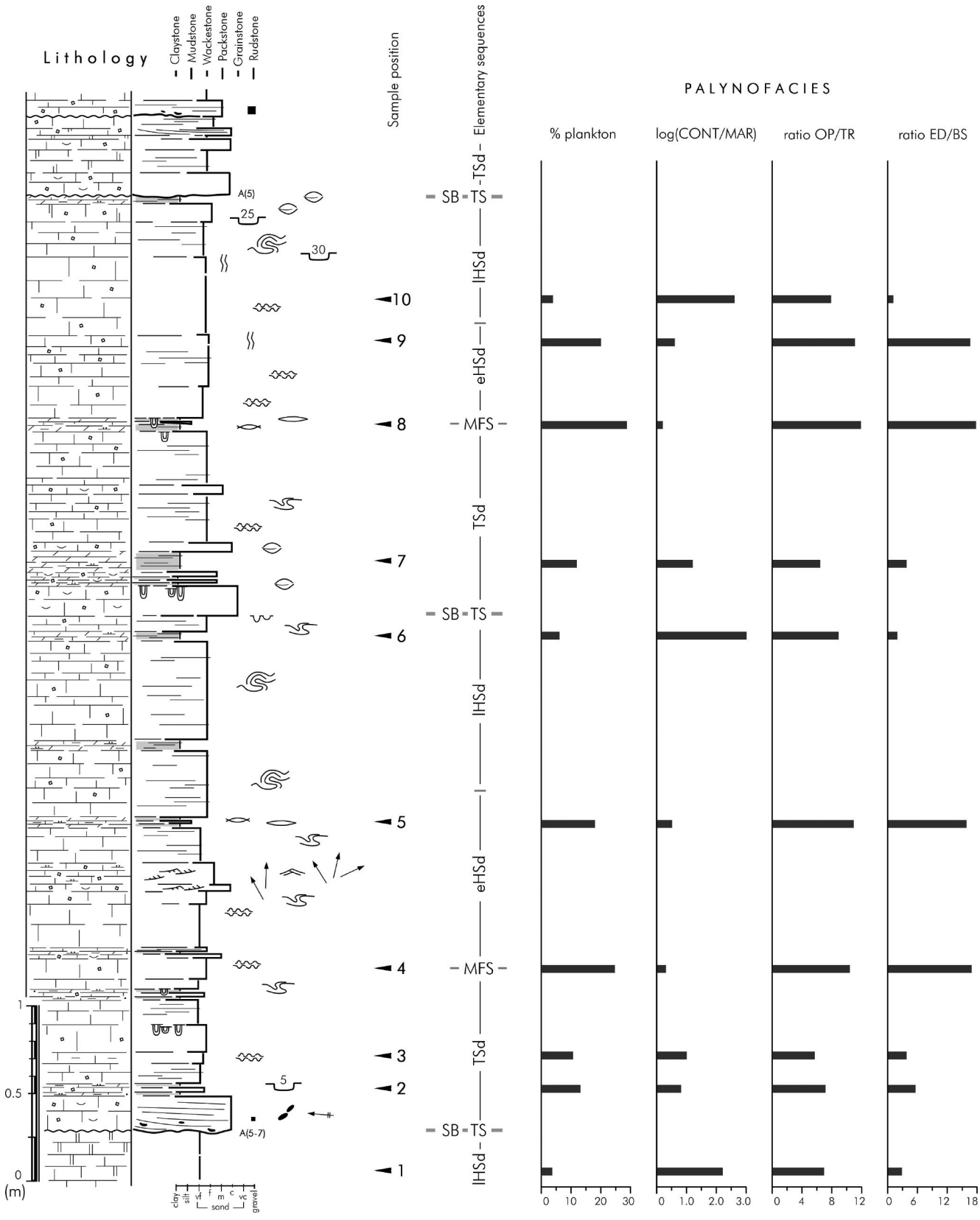

Fig. 10. Palynofacies patterns of elementary sequences 8 and 9 of the Opletnya Member (Fig. 3A, B). SB: sequence boundary; TS: transgressive surface; TSd: transgressive deposits; MFS: maximum-flooding surface; eHSd: early highstand deposits; lHSd: late highstand deposits. CONT: continental particles; MAR: marine particles; OP: opaque phytoclasts; TR: translucent phytoclasts; ED: equidimensional phytoclasts; BS: blade-shaped phytoclasts. The legend is as in Figure 3.

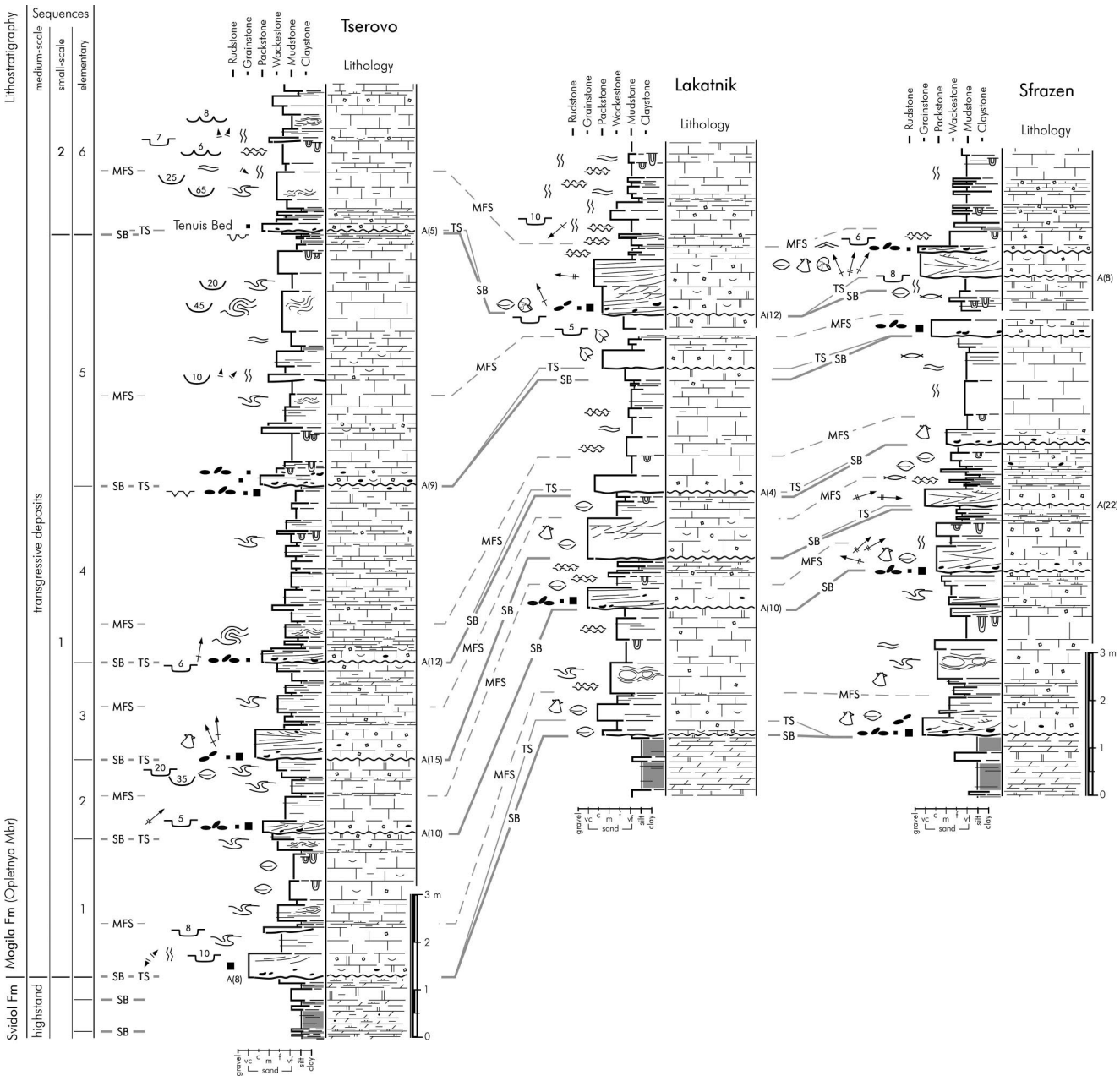

Fig. 11. Stratigraphic correlation of the first small-scale sequence of the Mogila Formation exposed in the Tserovo, Lakatnik and Sfrazen sections (logs of the latter two sections are from Ajdanlijsky *et al*., 2019). The legend and the numbering of the elementary sequences are as in Figure 3.

measured in pack- and grainstones documenting transgressive deposits, is an indicator of the ramp morphology with a slope to the south. The north-dominated, onshore direction of sedimentary transport was also noted as characteristic for the transgressive parts of other sections studied in the Iskar River gorge area (Ajdanlijsky *et al.*, 2019).

The ramp morphology is also documented by the variety of syndepositional soft-sediment deformation, which is much more frequent and intensive in the lower part of the Tserovo section, below the Sfrazen Bed. Complex, metre-thick, stacked slump units with prominent shear surfaces are recorded there, comprising small-scale folding, ball-and-pillow, and sigmoidal structures. The orientation of the sigmoidal structures reveals an almost equal pattern (NNE–SSW), indicating a slope, steepening towards the south. The present study confirms the relatively local, lateral development and the dominance of small-scale, sigmoidal structures in the upper, highstand part of elementary sequences, as noted in other sections of the area (Ajdanlijsky *et al.*, 2019). Moreover, on a large scale, such soft-sediment deformation structures with amplitudes over 40 cm are developed exclusively within early to late highstand deposits of the medium-scale sequences. This would indicate that during sea-level highstands, the soft sediment bodies prograded towards the south.

The enigmatic sigmoidal structures sometimes have been interpreted as tsunamites or as seismites (e.g., Michalik, 1997; Chatalov, 2001a, b, 2004). However, the position

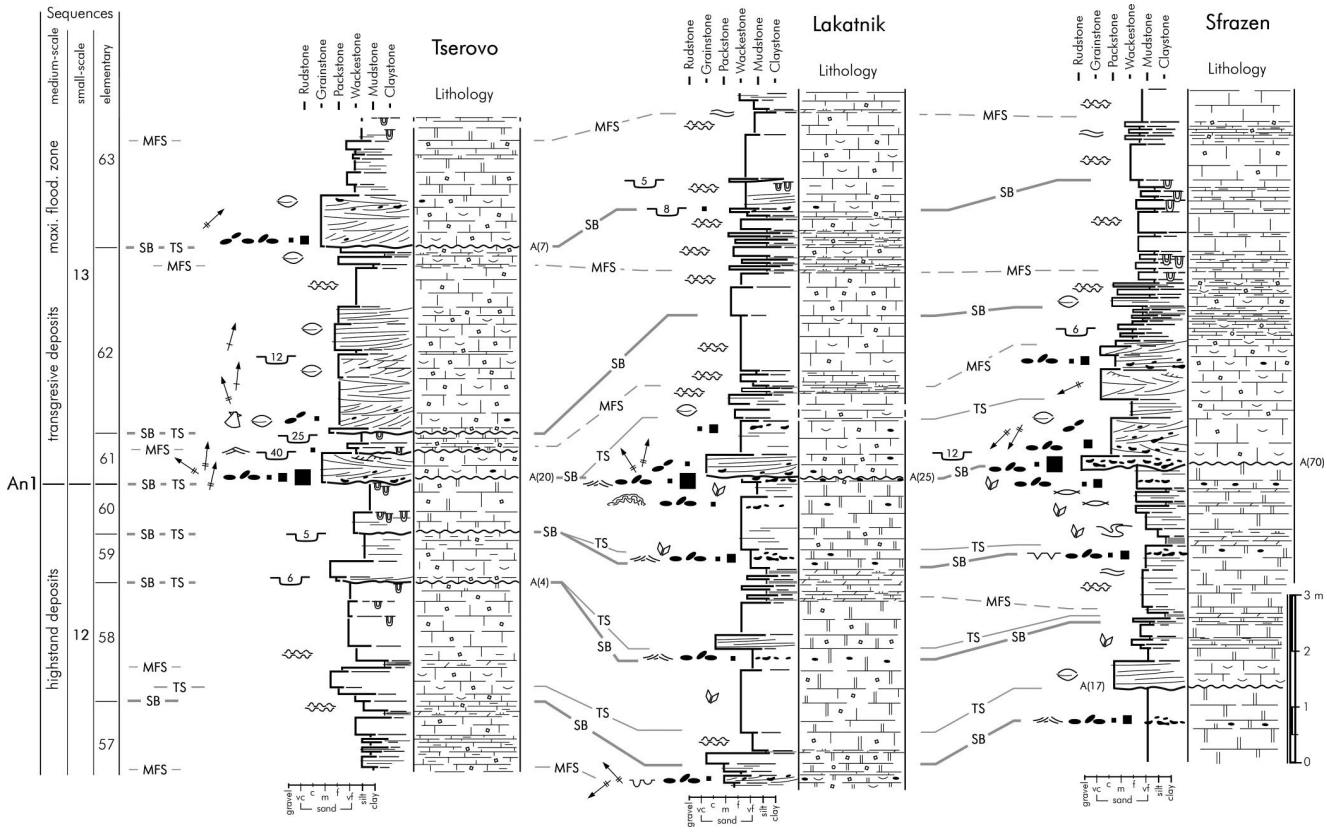

Fig. 12. Stratigraphic correlation of the An1 boundary detected in the Tserovo, Lakatnik and Sfrazen sections (logs of the latter two sections are from Ajdanlijsky *et al.*, 2019). The legend and the numbering of the elementary sequences are as in Figure 3.

of these structures in the stratigraphic record is commonly related to highstand deposits, while seismites or tsunamites would occur sporadically in any type of deposit. The interpretation as palaeoenvironmental indicators of highstand deposits as proposed by Ajdanlijsky *et al.* (2019) is thus supported by the new data from the Tserovo section. Nevertheless, a more detailed stratigraphic analysis of the Triassic ramp systems, previously seen as located in regions of strong seismic activity, should be carried out, differentiating carefully between local, regional, seismic, and sea-level induced features.

Cyclostratigraphic interpretation

The identification of three palynoassemblages (Ajdanlijsky *et al.*, 2019), placing the Olenekian-Anisian boundary in the uppermost Petrohan Terrigenous Group and the Aegean-Bithynian boundary within the upper Opletyna Member (Fig. 2), provides a stratigraphic scheme that allows estimation of the time duration of the Opletnya Member (Fig. 13). The major sequence boundary Ol4 (Olenekian 4; nomenclature according to Hardenbol *et al.*, 1998) is situated at the top of the Petrohan Terrigenous Group. Sequence boundary An1 (Anisian 1) has been identified at the major erosional surface between the thin elementary sequences 60 and 61 (Figs 3, 12), where accommodation was low and the facies imply very shallow, subtidal to supratidal conditions (evaporites) and reworking. These two boundaries bracket the Aegean succession, for which a time span of 1.6 Myr has been established (Li *et al.*, 2018; Ajdanlijsky *et al.*, 2019). Within this time span, 16 small-scale sequences have been identified, which means that one small-scale sequence represents 100 kyr and thus corresponds to the short orbital eccentricity cycle (Hinnov, 2018). In the Opletnya Member, 12 small-scale sequences are found up to sequence boundary An1 and two more above An1 that are situated in the Bithynian (Fig. 13).

Commonly, the small-scale sequences are composed of 5 elementary sequences, which consequently are interpreted as having formed in tune with the 20-kyr precession cycle (Hinnov, 2018). The orbital cycles translate into insolation changes, which – through complex feed-back processes – then influence climate and eustatic sea level (e.g., Strasser *et al.*, 1999; Strasser, 2018). Humid climatic conditions favour terrigenous run-off and thus the input of siliciclastics onto the ramp. Furthermore, autocyclic processes, such as the lateral migration of sediment bodies, commonly are superimposed on the orbitally controlled, allocyclic parameters. It is therefore not surprising that the elementary sequences are complex and do not always show a simple deepening-shallowing trend of facies (Fig. 3). They may contain erosion surfaces (e.g., elementary sequences 12, 15, and 22) that are here not interpreted as sequence boundaries related to eustatic sea-level falls but as being caused by local processes, such as channel migration or storm erosion. The combination of allo- and autocyclic processes is documented, for example, in the interval of the Sfrazen Bed in Tserovo (elementary sequences 31 to 37), which is also

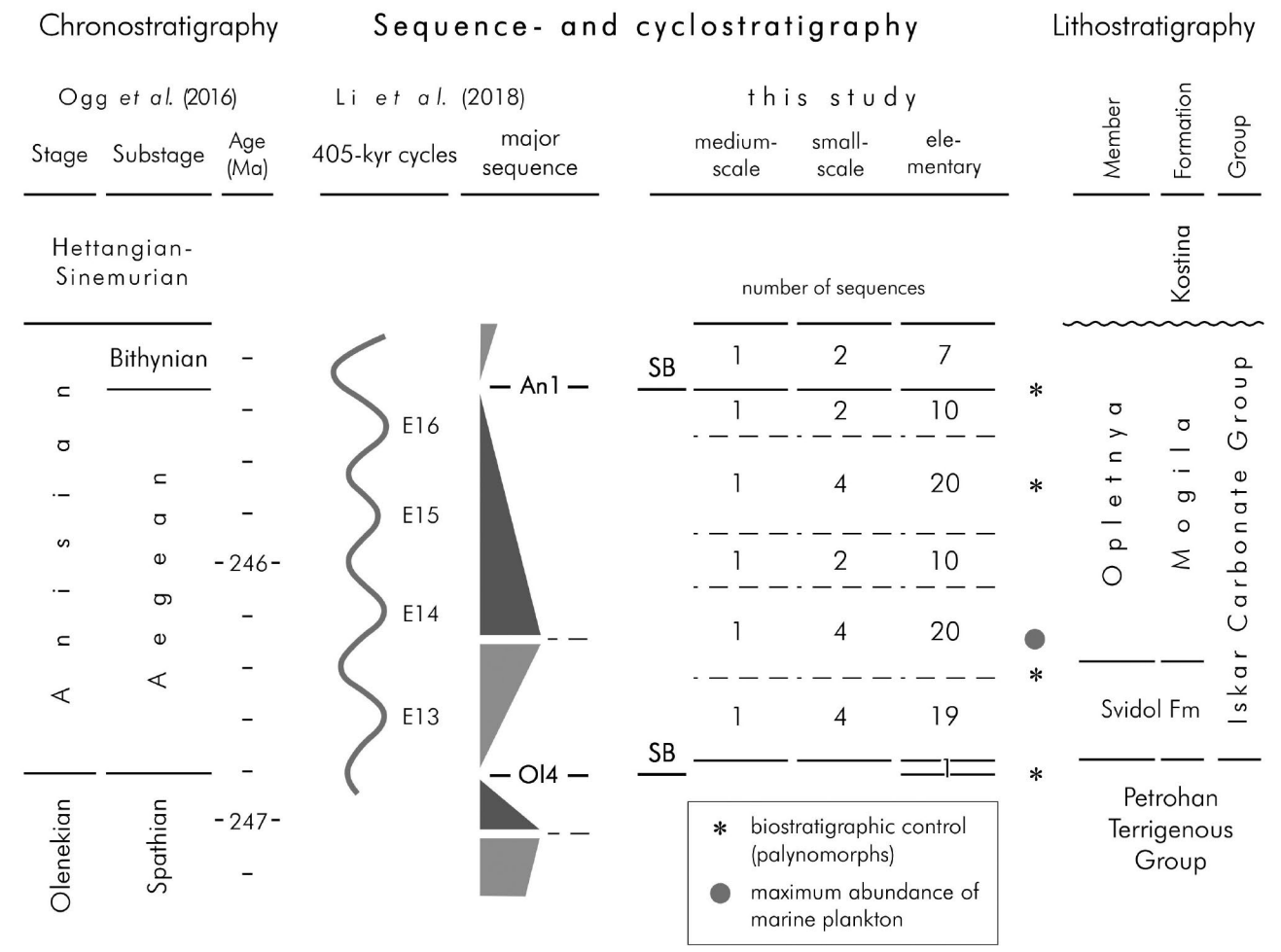

Fig. 13. Sequence- and cyclostratigraphic chart of the Opletnya Member in the studied Tserovo section. See text for explanation.

recognized in the same interval exposed in the Lakatnik section. In contrast, allocyclicity is prominent in the same interval of the Sfrazen section (Ajdanlijsky *et al.*, 2019).

The interpretation of the medium-scale sequences, comprising two or four small-scale sequences, is as yet undetermined. In South China, Li *et al.* (2018) identified four long eccentricity cycles (400 kyr; see also Hinnov, 2018) in the Aegean, while the present study documents five (Fig. 13). Most probably, this discrepancy results from a combination of allocyclic (e.g., Strasser *et al.*, 2000; Boulila *et al.*, 2008) and autocyclic processes, obscuring a clear signal of the long eccentricity cycle.

The comparison of the Tserovo section with the two northern sections (Ajdanlijsky *et al.*, 2019) shows the lateral variation of facies composition and thickness, while the number of sequences (i.e., recorded orbital cycles) within the succession is constant. This variation is interpreted as relating to the ramp morphology, which controlled water depth, clay content and the frequency, structure and intensity of syndepositional soft-sediment deformations.

The most prominent variations are changes in thickness of the elementary sequences within the small-scale sequences. The thicknesses of the first 6 small-scale sequences in Tserovo range between 2.9 and 5.8 m, i.e., almost twice those in the northern sections (ranging between 1.6 to 2.7 m). Upsection, within small-scale sequences 7 to 12, the thicknesses are almost identical in all sections, ranging between 1.3 and 2.0 m. The same trends were observed regarding the thickness of the small- and medium-scale sequences. The striking change in thickness pattern occurs at the base of the Sfrazen Bed, marking a prominent transgression in all sections. In Tserovo, in contrast to the other sections of the type area, the base of the Sfrazen Bed is not erosional, but associated with load casts and flame structures.

A major marine flooding phase is revealed by a distinct plankton peak (Fig. 13). The maximum abundance of marine acritarchs with 38% of the organic particles occurs in the lowermost Opletnya Member (within elementary sequences 8, which is part of the maximum-flooding zone of medium-scale sequence 1) and is interpreted to correspond to the maximum-flooding zone of the large-scale sequence Ol4 – An1 (Fig. 13).

Supra-regional correlations

A robust stratigraphic framework is essential for supra-regional correlations. The cyclicity of Anisian ramp systems along the northwestern Tethys margin has been described

from Hungary (Török, 1998; Götz *et al.*, 2003) and Poland (Jaglarz and Szulc, 2003; Götz *et al.*, 2005), where existing biostratigraphic schemes provide a reliable time frame. Götz and Török (2018) reviewed the cyclicity, described from Anisian ramps of the northwestern Tethyan and Peri-Tethyan realms, and proposed a high-resolution correlation. Matysik (2019) questions long-distance correlations, due to lateral facies heterogeneities of high-frequency depositional cycles in ramp settings, characterized by synsedimentary tectonics, such as the eastern Germanic realm of southern Poland. The ramp system of northwestern Bulgaria and its lateral extent have been recently discussed by Chatalov (2013, 2018). However, precise ages were not provided, due to the lack of biostratigraphic age control. With the recent palynological studies of Ajdanlijsky *et al.* (2018, 2019), the Olenekian–Anisian boundary and, including conodont data, the boundaries of the Anisian substages were identified in the uppermost Petrohan Terrigeneous Group and within the Mogila, Babino and Milanova formations of the lower Iskar Carbonate Group, respectively. Based on this stratigraphic framework, the timing of deposition can be estimated and cyclic hierarchies can be interpreted in the orbital Milankovitch frequency band. The precession and short eccentricity signals are very prominent, recorded as elementary and small-scale sequences, whereas the long eccentricity signal, documented in medium-scale sequences, is less prominent.

The use of marine plankton peaks for correlation of Tethyan and Peri-Tethyan sequences of different scales was highlighted by Götz and Török (2008). Plankton peaks of marine acritarchs, recorded in the early Anisian of northwestern Bulgaria, prove to be an additional correlation tool. In the present case, the maximum-flooding zone in the lowermost Opletnya Member correlates well with the maximum flooding proposed by Li *et al.* (2018) in South China (Fig. 13). Within elementary sequences, palynological signals are also recorded and thus regarded as a high-resolution correlation tool for future studies across the northwestern Tethys shelf.

CONCLUSIONS

A robust biostratigraphic, sequence-stratigraphic and cyclostratigraphic framework for the early Anisian (Aegean) ramp deposits of NW Bulgaria is established. Detailed analysis of facies and sedimentary structures allows the definition of depositional sequences on three levels (elementary, small-scale and medium-scale), which are hierarchically stacked and can be traced laterally between sections. According to the chronostratigraphic framework that assigns a duration of 1.6 Myr to the Aegean, it is implied that the elementary sequences formed in tune with the 20-kyr orbital precession cycle and that the small-scale sequences were controlled by the 100-kyr short eccentricity cycle. The medium-scale sequences are difficult to interpret, but some could have been influenced by the 400-kyr long eccentricity cycle. This cyclostratigraphy enables high-resolution correlation across the ramp.

The facies and sedimentary structures observed all indicate shallow-marine to peritidal depositional environments. However, important lateral variations were observed, which are attributed to the ramp morphology and to autocyclic processes, superimposed on the allocyclic, orbitally controlled sea-level changes. The study of sedimentary organic matter (more marine *versus* more terrigenous) complements the sedimentological and cyclostratigraphic interpretation. Moreover, the orientation of palaeotransport direction and common syndepositional deformation in the lower part of the succession reflects the ramp morphology, with a slope to the south. The results presented here are crucial for lateral correlation within the distinct ramp system of NW Bulgaria and for supra-regional correlation of the Anisian ramp systems in the northwestern Tethyan realm.

Acknowledgements

We acknowledge Petar Nikov and Fabio Sheitanov for their enthusiastic support during field work, Dimitar Tronkov for his critical remarks on Triassic stratigraphy, Elias Samankassou for discussion in the field, and Antonio Lakov for his comments on the mechanisms of syndepositional soft-sediment deformation. Our special thanks go to Alexandar Zdravkov for taking the microphotographs of thin sections in his petrographic lab at the Department of Geology and Exploration of Mineral Resources, University of Mining and Geology "St. Ivan Rilski", Sofia. The reviews by János Haas and Tadeusz Peryt and suggestions of the editors Michał Gradziński and Alfred Uchman are gratefully acknowledged. This study is part of the Triassic Ocean Project TRIO, led by A. E. Götz.

REFERENCES

Adams, A., Diamond, L. W. & Aschwanden, L., 2018. Dolomitization by hypersaline reflux into dense groundwaters as revealed by vertical trends in strontium and oxygen isotopes: upper Muschelkalk, Switzerland. *Sedimentology*, 66: 362–390.

Ajdanlijsky, G., Götz, A. E. & Strasser, A., 2018. The Early to Middle Triassic continental–marine transition of NW Bulgaria: Sedimentology, palynology and sequence stratigraphy. *Geologica Carpathica*, 69: 129–148.

Ajdanlijsky, G., Strasser, A. & Götz, A. E., 2019. Integrated bio- and cyclostratigraphy of Middle Triassic (Anisian) ramp deposits, NW Bulgaria. *Geologica Carpathica*, 70: 325–354.

Boulila, S., Galbrun, B., Hinnov, L. A. & Collin, P.-Y., 2008. High-resolution cyclostratigraphic analysis from magnetic susceptibility in a Lower Kimmeridgian (Upper Jurassic) marl-limestone succession (La Méouge, Vocontian Basin, France). *Sedimentary Geology*, 203: 54–63.

Budurov, K., Zagorchev, I., Trifonova, E. & Petrunova, L., 1997. The Triassic in Eastern Stara planina Mts. Lithostratigraphic notes. *Review of the Bulgarian Geological Society*, 58: 101–110.

Čatalov, G. & Visscher, H., 1990. Palynomorphs from Stoilovo Formation, Veleka Group (Triassic), Strandža Mountain, Southeast Bulgaria. *Geologica Balcanica*, 20: 53–57.

Catuneanu, O., 2019. Scale in sequence stratigraphy. *Marine and Petroleum Geology*, 106: 128–159.

Catuneanu, O., Abreu, V., Bhattacharya, J. P., Blum, M. D., Dalrymple, R. W., Eriksson, P. G., Fielding, C. R., Fisher, W. L., Galloway, W. E., Gibling, M. R., Giles, K. A., Holbrook, J. M.,

Jordan, R., Kendall, C. G. S. C., Macurda, B., Martinsen, O. J., Miall, A. D., Neal, J. E., Nummedal, D., Pomar, L., Posamentier, H. W., Pratt, B. R., Sarg, J. F., Shanley, K. W., Steel, R. J., Strasser, A., Tucker, M. E. & Winker, C., 2009. Towards the standardization of sequence stratigraphy. *Earth-Science Reviews*, 92: 1–33.

Chatalov, A., 2001a. Deformational structures in the Iskar Carbonate group (Lower–Upper Triassic) from the Western Balkanides. *Geologica Balcanica*, 30: 43–57.

Chatalov, A., 2001b. Signature of paleoseismic activity in the Triassic carbonate rocks from Northwestern Bulgaria. In: Gaupp, R. & Van der Klaw, S. (eds), *Sediment 2001: Programm, Kurzfassungen, Exkursionsführer. Schriftenreihe der Deutschen Geologischen Gesellschaft*, 13: 29.

Chatalov, A., 2004. Route VIII. Sedimentological sites in the carbonate Triassic between Lakatnik railway station and Opletnya village. In: Sinnyovsky, D. (ed.), *Geological Routes in the Northern Part of the Iskar River Gorge.* Vanio Nedkov Publishing House, Sofia, pp. 102–116.

Chatalov, A., 2013. A Triassic homoclinal ramp from the Western Tethyan realm, Western Balkanides, Bulgaria: Integrated insight with special emphasis on the Anisian outer to inner ramp facies transition. *Palaeogeography, Palaeoclimatology, Palaeoecology*, 386: 34–58.

Chatalov, A., 2018. Global, regional and local controls on the development of a Triassic carbonate ramp system, Western Balkanides, Bulgaria. *Geological Magazine*, 155: 641–673.

Dunham, R. J., 1962. Classification of carbonate rocks according to depositional texture. *AAPG Memoir*, 1: 108–121.

Götz, A. E., Szulc, J. & Feist-Burkhardt, S., 2005. Distribution of sedimentary organic matter in Anisian carbonate series of S Poland: evidence of third-order sea-level fluctuations. *International Journal of Earth Sciences*, 94: 267–274.

Götz, A. E. & Török, Á., 2008. Correlation of Tethyan and Peri-Tethyan long-term and high-frequency eustatic signals (Anisian, Middle Triassic). *Geologica Carpathica*, 59: 307–317.

Götz, A. E. & Török, Á., 2018. Muschelkalk ramp cycles revisited. In: Montenari, M. (ed.), *Stratigraphy and Timescales. Cyclostratigraphy and Astrochronology.* Academic Press, Amsterdam, pp. 265–284.

Götz, A. E., Török, Á., Feist-Burkhardt, S. & Konrád, Gy., 2003. Palynofacies patterns of Middle Triassic ramp deposits (Mecsek Mts., S Hungary): A powerful tool for high-resolution sequence stratigraphy. *Mitteilungen der Gesellschaft für Geologie- und Bergbaustudenten in Österreich*, 46: 77–90.

Gonzalez, R. & Eberli, G. P., 1997. Sediment transport and bedforms in a carbonate tidal inlet; Lee Stocking Island, Exumas, Bahamas. *Sedimentology*, 44: 1015–1030.

Hardenbol, J., Thierry, J., Farley, M., Jacquin, T., de Graciansky, P.-C. & Vail, P., 1998. Mesozoic and Cenozoic sequence chronostratigraphic framework of European basins. *SEPM Special Publication*, 60; chart.

Hardie, L. A. & Garrett, P., 1977. General environmental setting. In: Hardie, L. A. (ed.), *Sedimentation on the Modern Carbonate Tidal Flats of Northwest Andros Island, Bahamas. The Johns Hopkins University Studies in Geology*, 22: 12–49.

Hardie, L. A. & Ginsburg, R. N., 1977. Layering; the origin and environmental significance of lamination and thin bedding. In: Hardie, L. A. (ed.), *Sedimentation on the Modern Carbonate Tidal Flats of Northwest Andros Island, Bahamas. The Johns Hopkins University Studies in Geology*, 22: 50–123.

Hillgärtner, H., Dupraz, C. & Hug, W., 2002. Microbially induced cementation of carbonate sands: are micritic meniscus cements good indicators of vadose diagenesis? *Sedimentology*, 48: 117–131.

Hinnov, L. A., 2018. Cyclostratigraphy and astrochronology in 2018. In: Montenari, M. (ed.), *Stratigraphy and Timescales. Cyclostratigraphy and Astrochronology.* Academic Press, Amsterdam, pp. 1–80.

Ivanov, Zh., 1998. Tektonika na Balgaria. [Tectonics of Bulgaria]. Unpublished habil. thesis, Sofia University "St. Kliment Ohridski", 634 pp. [In Bulgarian.]

Jaglarz, P. & Szulc, J., 2003. Middle Triassic evolution of the Tatricum sedimentary basin: an attempt of sequence stratigraphy to the Wierchowa Unit in the Polish Tatra Mountains. *Annales Societatis Geologorum Poloniae*, 73: 169–182.

Kalvacheva, R. K. & Čatalov, G. A., 1974. Palynomorphen aus phyllitoiden Tonschiefern des Strandza-Gebirges. *Comptes Rendus de l'Académie Bulgare des Sciences*, 27: 1419–1422.

Li, M., Huang, C., Hinnov, L., Chen, W., Ogg, J. & Tian, W., 2018. Astrochronology of the Anisian stage (Middle Triassic) at the Guandao reference section, South China. *Earth and Planetary Science Letters*, 482: 591–606.

Lukoczki, G., Haas, J., Gregg, J. M., Machel, H. G., Kele, S. & John, C. M., 2019. Multi-phase dolomitization and recrystallization of Middle Triassic shallow marine-peritidal carbonates from the Mecsek Mts. (SW Hungary), as inferred from petrography, carbon, oxygen, strontium and clumped isotope data. *Marine and Petroleum Geology*, 101: 440–458.

Matysik, M., 2019. High-frequency depositional cycles in the Muschelkalk (Middle Triassic) of southern Poland: Origin and implications for Germanic Basin astrochronological scales. *Sedimentary Geology*, 383: 159–180.

Michalík, J., 1997. Tsunamites in a storm-dominated Anisian carbonate ramp (Vysoká Formation, Malé Karpaty Mts., Western Carpathians). *Geologica Carpathica*, 48: 221–229.

Montañez, I. A. & Osleger, D. A., 1993. Parasequence stacking patterns, third-order accommodation events, and sequence stratigraphy of Middle to Upper Cambrian platform carbonates, Bonanza King Formation, southern Great Basin. *AAPG Memoir*, 57: 305–326.

Montenat, C., Barrier, P., Ott d'Estevou, P. & Hibsch, C., 2007. Seismites: An attempt at critical analysis and classification. *Sedimentary Geology*, 196: 5–30.

Petrash, D. A., Bialik, O. M., Bontognali, T. R. R., Vasconcelos, C., Roberts, J. A., McKenzie, J. A. & Konhauser, K. O., 2017. Microbially catalyzed dolomite formation: From near-surface to burial. *Earth-Science Reviews*, 171: 558–582.

Petrunova, L., 1992a. First palynological evidence of the Ladinian Age of the Preslav Formation in Northwest Bulgaria. *Geologica Balcanica*, 22: 46.

Petrunova, L., 1992b. Palynological evidence of the Early Karnian Age of the Moesian Group in Northwest Bulgaria. *Geologica Balcanica*, 22: 94.

Petrunova, L., 1999. Palynological correlations of the Preslav Formation (Iskur Carbonate Group) to the Peri-Tethyan Triassic of Central Europe. *Geologica Balcanica*, 29: 136.

Petrunova, L., 2000. Palynomorphs around the boundary Lower-Middle Triassic from an olistolith in Eastern Stara Planina Mountains, Bulgaria. In: Grădinaru, E. (ed.), *Proceedings of the International Workshop on the Lower–Middle Triassic (Olenekian–Anisian) Boundary.* Tulcea, Romania, pp. 53–55.

Posamentier, H. W., Allen, G. P. & James, D. P., 1992. High-resolution sequence stratigraphy – the East Coulee delta, Alberta. *Journal of Sedimentary Petrology*, 62: 310–317.

Reineck, H.-E. & Singh, I. B., 1975. *Depositional Sedimentary Environments*. Springer, Berlin, 439 pp.

Strasser, A., 2018. Cyclostratigraphy of shallow-marine carbonates – limitations and opportunities. In: Montenari, M. (ed.), *Stratigraphy and Timescales. Cyclostratigraphy and Astrochronology.* Academic Press, Amsterdam, pp. 151–187.

Strasser, A., Hillgärtner, H., Hug, W. & Pittet, B., 2000. Third-order depositional cycles reflecting Milankovitch cyclicity. *Terra Nova*, 12: 303–311.

Strasser, A., Pittet, B., Hillgärtner, H. & Pasquier, J.-B., 1999. Depositional sequences in shallow carbonate-dominated sedimentary systems: concepts for a high-resolution analysis. *Sedimentary Geology*, 128: 201–221.

Török, Á., 1998. Controls on development of Mid-Triassic ramps: examples from southern Hungary. In: Wright, V. P. & Burchette, T. P., (eds), *Carbonate Ramps. Geological Society London, Special Publication*, 149: 339–367.

Tronkov, D., 1968. Die Grenze Untere Trias–Mittlere Trias in Bulgarien. *Bulletin of the Geological Institute of the Bulgarian Academy of Science, Paleontological Series*, 17: 113–130. [In Bulgarian, with German summary.]

Tronkov, D., 1981. Stratigraphy of the Triassic System in part of the Western Srednogorie (West Bulgaria). *Geologica Balcanica*, 11: 3–20. [In Russian, with English summary.]

Tronkov, D., 1983. Stratigraphic problems of Iskar Carbonate Group (Triassic) in South-western Bulgaria. *Geologica Balcanica*, 13: 91–100. [In Russian, with English summary.]

Wood, G. D., Gabriel, A. M. & Lawson, J. C., 1996. Palynological techniques – processing and microscopy. In: Jansonius, J. & McGregor, D. C. (eds), *Palynology: Principles and Applications. AASP Foundation*, 1: 29–50.

Yanev, S., 2000. Palaeozoic terranes of the Balkan Peninsula in the framework of Pangea assembly. *Palaeogeography, Palaeoclimatology, Palaeoecology*, 161: 151–177.